Elsevier Editorial System(tm) for Marine and Petroleum Geology
Manuscript Draft

Manuscript Number:

Title: Acoustic properties in continental carbonates and their relation to depositional environments, porosity and pore types

Article Type: Full Length Article

Keywords: Continental carbonate; acoustic-wave velocity; pore type

Corresponding Author: Mr. Jeroen Johan Soete, Ph.D

Corresponding Author's Institution: KU Leuven

First Author: Jeroen Johan Soete, Ph.D

Order of Authors: Jeroen Johan Soete, Ph.D; Luuk M Kleipool, Ph.D; Hannes Claes, Ph.D; Steven Claes, Ph.D; Helen Hamaekers, Ph.D; Sandor Kele, Dr.; Mehmet Özkul, Prof. Dr.; Anneleen Foubert, Prof. Dr.; John J Reijmer, Prof. Dr.; Rudy Swennen, Prof. Dr.

Abstract: Abstract - Sonic velocities were measured under variable confining pressures (5 - 10 - 20 - 40MPa) of Pleistocene continental carbonates, originating from quarries near Denizli (Turkey) and Süttő and Budakalász (Hungary). Combined with other petrophysical properties (porosity, permeability and density) and petrographical characteristics (facies, fabric, texture and diagenesis) of the individual samples, insight is gained in the parameters controlling compressional-wave (Vp) and shear-wave velocities (Vs) of these precipitates. At 40 MPa confining pressures, Vp ranges between 3695 and 6097m/s and Vs from 2037 to 3140m/s. Velocity variations in continental carbonates are primarily linked to sample heterogeneity, i.e. differences in fabric, texture and porosity, and are not related related to changes in mineralogy or composition. Body wave velocities have a positive correlation with sample density and an inverse correlation with porosity. However, measured departures from the regression line can amount to about 900m/s and are linked to variations in pore types and shapes. The latter were typified using micro-computerized tomography (μCT) rendered pore volumes. Samples with over 50 vol% mouldic porosity (macropores) show faster wave propagation than expected from their total porosities. The rigid frame and micrite surrounding the patchy distributed moulds will cause the high velocities. Samples dominated by interlayer, intercrystalline and interparticle porosity (micro- and mesopores) have a more uniform pore distribution and scattering of the wave front causes wave attenuation. The measured continental carbonates, despite being sampled at three different locations, define a specific compressional-wave velocity (y-axis) versus porosity (x-axis) equation, i.e. ($\log(y) = -0.0048x + 3.7844$) that differs from the Vp-porosity paths defined by marine carbonates. The study demonstrates how seismic sections in continental carbonate systems can contain seismic reflectors that are not caused by non-carbonate intercalations, but relate to geobody boundaries, in which the seismic expression is function of porosity and pore types. This study provides insight in the petrophysical properties, i.e. porosity, permeability and acoustic velocities of continental carbonates and is of high importance for the acoustic modeling in subsurface continental carbonate reservoirs.

Suggested Reviewers: Philippe Leonide Dr.
Postdoc, Carbonate team GSRC, Université de Provence Université de Provence (Marseille, France)
philippe.leonide@univ-provence.fr

Flavio Anselmetti Prof. Dr.
Professor, Institute of Geological Sciences, University of Bern
flavio.anselmetti@geo.unibe.ch

Mathieu Pellerin
R&D Carbonate, Total
matthieu.pellerin@ep.total.no

Gregor Eberli Prof. Dr.
Professor, Marine Geology and Geophysics, University of Miami
g.eberli@miami.edu

Cover Letter

February 7, 2014-02-07

Dear Mr./Mrs.,

Together with this letter we submit a manuscript entitled “Acoustic properties in continental carbonates and their relation to depositional environments, porosity and pore types“, by Soete et al. We would like to have the manuscript considered for publication as a full length article in Marine and Petroleum Geology.

To our knowledge, this is the first report showing acoustic velocities in continental, calcareous spring carbonates and relating these velocities to depositional environments, porosity and pore types. The research is in line with industry projects that study reservoir analogues and their architectures. We therefore believe our findings would appeal to the readership of Marine and Petroleum Geology. We confirm that this manuscript has not been published elsewhere and is not under consideration by another journal. All authors, listed in the text, have approved the manuscript and agree with its submission.

Please address all correspondence to:

Jeroen Soete - PhD Student
Geology - Carbonate Sedimentology and Petrophysics
Department of Earth & Environmental Sciences
Katholieke Universiteit Leuven
Celestijnenlaan 200E
B-3001 Heverlee, Belgium
TEL: +32(0)16 32 77 96
E-mail: jeroen.soete@ees.kuleuven.be

We look forward to hearing from you at your earliest convenience.

With my best regards,
Jeroen Soete

Highlights

- Acoustic velocities were measured in 60 continental carbonate plugs.
- Acoustic velocity is dependent on pore types, pore size and distribution.
- Seismic reflectors relate to geobody boundaries.
- Relations of acoustic velocity in marine and continental carbonates were examined.
- Velocity decrease in continental carbonates is slower with increasing porosity.

Acoustic properties in continental carbonates and their relation to depositional environments, porosity and pore types

Soete, J.[a], Kleipool, L.M.[b], Claes, H.[a], Claes, S.[a], Hamaekers, H.[a], Kele, S.[c,d], Özkul, M.[e], Foubert, A.[f], Reijmer, J.J.G. [b], Swennen, R.[a]

[a]Geology, Department of Earth and Environmental Sciences, KU Leuven, Celestijnenlaan 200E, 3001 Heverlee, Belgium (e-mail: jeroen.soete@ees.kuleuven.be, telephone: +32 16 32 77 96).

[b]Faculty of Earth and Life Sciences, Sedimentology and Marine Geology, VU University Amsterdam, De Boelelaan 1085, Amsterdam, The Netherlands.

[c]Institute for Geochemical Research, Hungarian Academy of Sciences, 1112 Budapest, Budaörsi út 45, Hungary.

[d]ETH Zurich, Sonneggstrasse 5, 8092 Zürich, Switzerland

[e]Department of Geological Engineering, Pamukkale University, TR–20070, Denizli, Turkey.

[f]Department of Geosciences, Université de Fribourg, Chemin du Musée 6, 1700 Fribourg, Switzerland.

Abstract – Sonic velocities were measured under variable confining pressures (5 – 10 – 20 – 40MPa) of Pleistocene continental carbonates, originating from quarries near Denizli (Turkey) and Süttő and Budakalász (Hungary). Combined with other petrophysical properties (porosity, permeability and density) and petrographical characteristics (facies, fabric, texture and diagenesis) of the individual samples, insight is gained in the parameters controlling compressional-wave (V_p) and shear-wave velocities (V_s) of these precipitates. At 40 MPa confining pressures, V_p ranges between 3695 and 6097m/s and V_s from 2037 to 3140m/s. Velocity variations in continental carbonates are primarily linked to sample heterogeneity, i.e. differences in fabric, texture and porosity, and are not related related to changes in mineralogy or composition. Body wave velocities have a positive correlation with sample density and an inverse correlation with porosity. However, measured departures from the regression line can amount to about 900m/s and are linked to variations in pore types and shapes. The latter were typified using micro-computerized tomography (µCT) rendered pore

volumes. Samples with over 50 vol% mouldic porosity (macropores) show faster wave propagation than expected from their total porosities. The rigid frame and micrite surrounding the patchy distributed moulds will cause the high velocities. Samples dominated by interlayer, intercrystalline and interparticle porosity (micro- and mesopores) have a more uniform pore distribution and scattering of the wave front causes wave attenuation. The measured continental carbonates, despite being sampled at three different locations, define a specific compressional-wave velocity (y-axis) versus porosity (x-axis) equation, i.e. ($\log(y) = -0.0048x + 3.7844$) that differs from the V_p-porosity paths defined by marine carbonates. The study demonstrates how seismic sections in continental carbonate systems can contain seismic reflectors that are not caused by non-carbonate intercalations, but relate to geobody boundaries, in which the seismic expression is function of porosity and pore types. This study provides insight in the petrophysical properties, i.e. porosity, permeability and acoustic velocities of continental carbonates and is of high importance for the acoustic modeling in subsurface continental carbonate reservoirs.

Key words: Continental carbonate; acoustic-wave velocity; pore type

1. Introduction

Continental carbonate deposits gained recent interest due to their potential as reservoir rocks, e.g. the supergiant fields in the Middle East (Nurmi & Standen, 1997) and offshore Brazil (Aslanian et al., 2009; Sant'Anna et al., 2004; Thompson & Oftebro, 2011). The genesis of continental carbonates is associated with physico-chemical and biological precipitation that largely influences the rock texture and petrophysical properties (Toumelin et al., 2003). This causes petrophysical heterogeneity that can become even more pronounced due to diagenetic overprinting (with cementation, dissolution, recrystallisation, dolomitisation, fracturing, etc.). Continental carbonates can form in a thin waterfilm in sub-aerial conditions, or in lake, marsh and fluvial environments. Samples in this study are calcareous spring deposits, associated with ambient and hydrothermal fluids (El Desouky et

al.,submitted; Sierralta et al., 2010). Their deposition is controlled by a complex interplay of physico-chemical, biological and hydrological factors, including CO_2 degassing, presumably the dominating process for continental carbonate precipitation around the globe (Fouke, 2011; Guo & Riding, 1998; Kele et al., 2011; Özkul et al., 2013; Özkul et al., 2014; Pentecost, 2005). Continental carbonates have been widely studied (Alonso-Zarza & Tanner, 2010; Ford & Pedley, 1996; Pedley & Rogerson, 2010; Pentecost, 2005), however, a detailed investigation of the rock petrophysics was seldom accomplished. This paper investigates the behaviour of acoustic waves in continental carbonates and addresses the question whether acoustic analyses are helpful for carbonate rock typing purposes.

The dependency of sonic velocities on lithology, rock texture and fabric is the key to understand acoustic logs and seismic sections in sedimentary systems. Compressional-wave velocity and bulk density are used to calculate acoustic impedance. In carbonate lithologies that consist purely of calcite, the grain density variations are limited, meaning that other parameters must cause variations in body wave velocity. These parameters are of importance for the interpretation of seismic reflectors and geophysical data. The control that is exhibited by porosity on acoustic velocity was already reported in the late fifties (Biot, 1956; Gassman, 1951). Causes for velocity variations in pure carbonates were part of several studies especially from the early nineties onwards. It was concluded that not only porosity, but also the entire rock fabric and its texture are of importance (Anselmetti & Eberli, 1993; Wang et al., 1991). Moreover, carbonates are prone to diagenesis, which can easily alter porosity, crystal morphology, the rigidity of the solid framework, etc. (Anselmetti & Eberli, 1993; Braaksma et al., 2003; Verwer et al., 2008). In this study, compressional-wave velocity (V_p) and shear-wave velocity (V_s) are measured on continental carbonate samples from three different areas, under confining pressures that approach in situ subsurface conditions. Samples originate from four different sedimentological facies-types, namely the sub-horizontal, reed, cascade and waterfall facies. Sonic velocity measurements were done in combination with petrography, X-Ray Diffraction (XRD) and µCT analyses.

2. Geological setting

The selected dataset of Quaternary continental carbonates is assembled from quarries near Denizli, in Turkey and from Süttő (Bakacsi et al., 1994; Sierralta et al., 2010) and Budakalász (Kele et al., 2003) in Hungary.

The Denizli Basin (Western Turkey) is a Neogene-Quaternary depression, of 70 by 50 km. The basin is the continuation of the E–W-trending Büyük Menderes Graben and the NW–SE-trending Gediz Graben (Bozkurt & Bozkurt, 2009; Gürer & Yilmaz, 2002; Kele et al., 2011; Özkul et al., 2002; Özkul et al., 2013). The Quaternary deposits are separated from the older stratigraphic units by an angular unconformity. Conglomerate, sandstone and mudstone are found in the Quaternary succession. The deposits from this geological period are subdivided in the Tosunlar Formation, with alternating conglomerate, sand- and mudstone deposits, and alluvial fan deposits of the uppermost Quaternary. The alluvium strata are associated with continental carbonate deposits (Alçiçek et al., 2007). The continental carbonates (including the world heritage site of Pamukkale) are known to occur along the bounding normal faults of the Denizli Basin (figure 1A).

Topographic highs, such as horst structures, act as hydraulic heads along which meteoric water infiltrates (Özkul et al., 2013). The down going fluid circulates through the subsurface and dissolves Mesozoic carbonates. Strontium isotope analyses, both on bulk samples and crystalline cement bands have shown that the Lycian nappes (Mesozoic) are a likely candidate as source rock (El Desouky et al., submitted; Gundogan et al., 2008; Kele et al., 2011). Normal faulting activity in the area gave birth to both ambient and hot springs. The continental carbonate deposits examined in this study are situated in the Ballık area, at the junction of the locally E-W trending Denizli Graben and the adjacent NE-SW trending Baklan Graben (Van Noten et al., 2013). The sampling location for this

study is the Alimoğlu quarry (figure 1B), where cores (3.54 inch or 9 cm diameter) were drilled at each excavation level.

The Transdanubian Range (TR) is a horst structure in the Pannonian Basin, Hungary (Dolton, 2006; Haas, 2012). The succession of the TR starts off with Lower Paleozoic marine formations, followed by continental and shallow marine sediments from the Late Permian to Late Triassic. A large carbonate platform developed over the TR during the Late Triassic. The Buda Mountains and Gerecse Hills (figure 2) outcrop along the Danube River. They are part of the Transdanubian Range and are mainly comprised of Mesozoic carbonates, which are covered by Cenozoic clastic and carbonate sequences. The terrace region of the Danube River is characterised by alluvial deposits (sand and gravel), but often continental carbonate precipitates exists.

High topographic differences between meteoric recharge (Buda Mountains and Gerecse Hills) and discharge areas (incised river terraces of the River Danube) resulted in strong hydraulic gradients, which are the principal driving force for subsurface water circulation in the area. The above average geothermal gradient of the Pannonian basin, associated with an extensional setting and volcanic zones, are two important factors steering the thermal waters. Infiltrated and heated meteoric water can mix with for example karstic water, and form corrosive fluids that enhance carbonate dissolution. Surfacing of CO_2-rich, thermal fluids results in the precipitation of continental carbonates (Goldscheider et al., 2010; Nador, 1993; Sierralta et al., 2010). The Budakalász and Süttő continental carbonates, respectively from the Buda Mountains and Gerecse Hills are examples of deposits that cover geomorphical steps (terraces) of the Danube River. Cores (3.54 inch or 9 cm diameter) were taken in both quarries.

3. Methodology

The petrophysical measurements are conducted on sixty 1.5-inch (3.81 cm) diameter plugs, acquired by undercoring the whole core drillings with a Hilti water-cooled diamond coring drill. After plugging, the samples are cut and polished to make the ends flat and parallel. In the first step of the research, samples are sent to Panterra Geoconsultants (Leiderdorp, The Netherlands) for petrophysical (porosity and permeability) analyses. The effective porosity in the plugs is measured by means of helium expansion porosimetry. Gas permeability, in this case with nitrogen gas (N_2), is measured in a steady state permeameter.

XRD analysis of 10 representative samples provides an overview of the dominant minerals present in the analysed plug samples. 2.7 grams of the sample and 0.3 gram Zinc oxide (10%), the internal standard for XRD analyses, are mixed and placed in sample holders for quantitative XRD analysis. Measurements have been carried out with a Philips PW 1830 generator at 45kV and 30mA, using Cu-Kα-radiation and a scan speed of 0.010° 2ϑ/s. Diffraction patterns are subsequently compared against mineral patterns of a standard database in the DIFFRAC^{plus}, 2004, EVA software 10.0 rev. 1 (Bruker AXS). Quantitative analyses are carried out using the Rietveld method, with TOPAS-Academic V4.1 and JEdit V4.2 software packages (Coelho, 2012).

Ultrasonic wave velocities in the continental carbonate samples are measured to characterise their acoustic properties. Prior to the sonic velocity analysis, the plugs are dried at 65°C for at least three days to ensure that all water is removed from the samples. Even small amounts of water could significantly lower the elastic shear moduli and give cause to erroneous analyses data (Mavko et al., 2009). Next, samples are left to equilibrate for 48 hours at room temperature and humidity conditions (19-21°C, 50-60%).

Ultrasonic compressional-wave velocity (V_p) and shear-wave velocity (V_s) are measured with a High Pressure (ultrasonic) Measurement System (HPMS), as function of the applied confining pressure with a transducer arrangement (VerdeGeoscience©, Vermont, U.S.A.) that propagates one compressional and two independent and orthogonally shear waves (V_s1 and V_s2) along the core axis. The orthogonal shear-waves are averaged to produce a homogeneous shear-wave velocity. The experimental setup contains a source and receiver crystal. The source crystal is exited by a fast rise time electrical voltage pulse, producing a sonic pulse with a frequency of 1 MHz. The receiver crystal records the flight-time of the first arriving wave front of the sonic pulse (García-del-Cura et al., 2012). Acoustic velocities are obtained by measuring the one-way travel time along the sample axis divided by the sample length. The arrival time is picked when the signal exceeds a threshold of the first three half-cycles of the signal. The error range of the ultrasonic velocity measurements falls within 3%. The measurements were conducted at nine confining pressures, ranging between 0 and 40 MPa. The successive confining pressures at which the velocities are measured in one hysteresis loop are: 2.5, 5, 10, 20, 40 MPa on the prograde path and 40, 20, 10, 5 and 2.5 MPa on the retrograde path. The elastic moduli can be extracted from the velocity measurements and the sample density (Mavko et al., 2009), based on the following equations:

$$\boldsymbol{K = \rho\left(V_p^2 - \frac{4}{3}V_s^2\right)} \qquad [\boldsymbol{Eq.1}]$$

$$\boldsymbol{\mu = \rho V_s^2} \qquad [\boldsymbol{Eq.2}]$$

$$\nu = \frac{(V_p^2 - 2V_s^2)}{\boldsymbol{2(V_p^2 - V_s^2)}} \qquad [\boldsymbol{Eq.3}]$$

$$E = \frac{V_p^2 \rho (1+\nu)(1-2\nu)}{1-\nu} \qquad [Eq.4]$$

With K the bulk modulus (Equation 1), μ the shear modulus (Equation 2), ν the Poisson's ratio (Equation 3), E the Young's modulus (Equation 4) and ρ the density. The density of the plugs, both dry and bulk, are calculated from the dry and saturated weights in combination with the cylindrical volumes. The grain density of the samples is determined with an Micromeritics Accupic 1330 helium pycnometer and porosity (error-range of 1%) is subsequently calculated from dry and grain density (Anselmetti & Eberli, 1993; Kenter et al., 1997; Verwer et al., 2008).

Micro-Computer Tomography (μCT) scans of 10 samples, used in the acoustic velocity measurements, are subjected to a quantitative pore network analysis. The samples are scanned with a Phoenix Nanotom S machine (GE Measurement and Control Solutions, Wunstorf, Germany), equipped with a 180kV/15W high-performance nanofocus X-ray tube and a 2304 × 2304 pixel Hamamatsu detector. A voltage of 140kV and current of 280μA is applied to a tungsten target. A 0.3mm thick cupper filter is installed during the scans.

Radiographs are reconstructed with the Phoenix datos|x 2.0 reconstruction software (GE Measurement and Control Solutions, Wunstorf, Germany) and images with an isotropic voxel size of 16μm³ are exported. The slices are segmented and analysed in Matlab R2011b and Avizo Fire v.7 software. Pore shape parameters such as sphericity, roundness and form ratio (with L, assigned to the longest dimension of the pore, the parameter I assigned to the longest dimension perpendicular to L and S orthogonal to both L and I) are calculated based on the segmented CT images. A pore classification system (figure 3) based on these parameters is used to determine the volume percentages of different pore types in the CT scanned continental carbonate samples. This allows

estimating the share of individual pore shapes and pore types to the total porosity (Claes et al., 2013) and their potential effect on acoustic velocities.

4. Results

4.1. Geobody architecture, facies and petrography

Detailed line drawings were made of the accessible excavation levels in the quarries and revealed the sedimentary evolution of the deposits through time (figure 4). At both study sites, Turkey and Hungary, the excavated sequences start off with horizontal to sub-horizontal (inclinations not exceeding 5°) laminations. The lamination is apparent due to the millimetre to centimetre-scale alternation of white, white to beige and brownish layers and is accentuated by layer parallel porosity (pseudo-fenestral, interparticle and interlayer porosity), pronounced along laminae contacts. These characteristics make up the sub-horizontal facies (figure 4A).

The bryo- and macrophyte rich reed facies covers the sub-horizontal facies. Under optimal growth conditions (water depth, temperature turbulence, etc.) plants such as reed, grasses and bryophytes flourish and both in situ and eroded plant casts can be formed due to calcite encrustation and the subsequent decay of organic matter. Once a few plants have rooted, they facilitate further plant growth. Carbonate precipitates and trapped cements crenulate around plant structures and cause the development of low relief topographic features, i.e. phytoherm structures. Plant-mouldic porosity and phytoherm structures characterise the reed facies (figure 4B).

The progradational nature of the carbonate systems and the continued build-up creates topography. This topography initiates the precipitation of sloping dendritic crusts and peloidal micrites, the main components of the sloping cascade facies and which may or may not contain bryophytes and macrophytes (figure 4C). Pore types in between peloidal micrites and dendrite crusts can be similar to the sub-horizontal facies, i.e. pseudo-fenestral, inter- and intra-particle porosity. Areas containing

plant material, however, lead to mouldic porosity occurrences. Locally, steep waterfalls of several metres in height can develop. Plant-framework porosity, formed between complex networks of interfingering overcrusted plants, is characteristic for the waterfall systems. The plant frames can redirect the water flow and prevent precipitation in underlying cavities, resulting in sheltered porosity systems, with volumes up to >20m³ (figure 4D). Plant framework and shelter porosity can occur in the cascade facies, but are of limited importance to the pore network, which is in contrast to their role in the waterfall facies.

In depressions reworked carbonate material accumulates, giving rise to sub-horizontal deposits. Finally reeds containing sub-parallel bedded lithologies cover the continental carbonate system. Toward the flanks, green coloured marls frequently interfinger with the continental carbonates. The marls laterally may grade into polymict conglomerates (figure 4E). Different facies are associated with different pore types and even intrafacies variations in pore types and their distributions occur. The continental carbonate systems are heterogeneous and complex, and their more detailed sedimentological description can be found in Claes, et al. (Submitted).

4.2. Mineralogy

The analysed continental carbonates consist almost exclusively, nearly hundred percent, of calcite. Diffractograms clearly show the presence of zincite, the internal standard and calcite. Next to the dominant carbonate mineralogy, a minor presence of quartz can be deduced. Except for quartz, small amounts of amorphous phases, organic matter and clays occur in some of the samples. The amorphous phase cannot be analysed with XRD and the minor quantities of clay minerals make it difficult to determine their mineralogies more accurately. Aragonite, frequently observed in continental carbonates (Pentecost, 2005), is absent in the analysed samples.

4.3. Petrophysical properties

Sixty plugs of continental carbonate were analysed to assess the impact of rock fabric and texture on body wave propagation. Measured values of the dry density (ρ_d), grain density (ρ_g), porosity, P-wave velocity, S-wave velocity, V_p/V_s ratio and acoustic impedance data are given in table 1. ρ_d and ρ_g range from 1.77 to 2.57g/cm³ and 2.56 to 2.72g/cm³ respectively, yielding porosity values of 2.8 to 34.7% (mean value of 12.9%). The nearly perfect correlation, a correlation coefficient of 0.99, between different porosity measurements confirms the consistency of the individual measurements. Permeability data (figure 5) of the carbonates show a skewed distribution and a large range over several orders of magnitude, between 0.05 and 18.000mD. Carbonates, heterogeneous with complex primary fabrics and prone to diagenetic alteration (e.g. dissolution, cementation, recrystallisation, dolomitisation, etc.), generally contain complex pore networks that may complicate the relation between porosity and permeability parameters (Dewit et al., 2012; Lapponi et al., 2011; Nurmi & Standen, 1997). Porosity and permeability data of the samples appear therefore with large ranges and deviate strongly from a linear correlation.

4.4. Acoustic velocity measurements

Shear-wave velocity and compressional-wave velocity values are given for confining pressures of 40MPa, which simulate in situ subsurface pressure conditions. The continental carbonates display a wide range in velocities; V_p varies between 3695 and 6097m/s, and V_s between 2037 and 3140m/s. For a given sample, the V_s value is approximately 55% of the V_p value. The V_p versus V_p/V_s ratio plot (figure 6) is specifically included to show that V_p/V_s ratios range between 1.80 and 2. Hysteresis loops of the compressional-wave data illustrate, on the prograde path, an initial fast rise of the velocity, until a plateau is reached (in most cases around 10-20MPa). At this point, instable micropores and microfractures are closed and their effect on the V_p data is minimized. Some of the samples approach starting conditions towards the end of the hysteresis loop, the deformation is considered elastic (figure 7).

Table 1. Summary of the conducted petrophysical measurements

Sample	Facies	ρ_d (g/cc)	ρ_s (g/cc)	Accupyc ϕ (%)	Kl. Perm (mD)	V_p (40 Mpa) (m/s)	V_s (40 Mpa) (m/s)	A.I. (10^6 Ns/m³)
Al01	Pool	2,45	2,63	6,5	0,1	5440	2935	13,35
AL02	Pool	2,49	2,63	5,2	0,2	5482	2968	13,68
Al03	Pool	2,41	2,60	7,2	8,4	5619	2986	13,55
Al04	Pool	2,50	2,57	2,8	0,1	5620	3012	14,03
Al05	Casc.	2,34	2,61	10,5	1,7	5420	2911	12,67
Al06	Wfall.	1,80	2,72	33,6	14600,0	4075	2191	7,36
Al08	Reed	2,26	2,60	12,9	69,4	5628	2941	12,73
Al09	Reed	2,09	2,61	19,7	524,0	5253	2827	11,00
Al10	Pool	2,37	2,62	9,7	0,1	5690	2998	13,49
Al11	Pool	2,46	2,63	6,6	0,8	5710	3018	14,05
Al12	Pool	2,46	2,65	7,2	0,1	5561	2988	13,66
Al13	Wfall.	1,94	2,66	26,8	1116,0	4267	2312	8,30
Al14	Wfall.	1,87	2,68	30,0	1611,0	4162	2182	7,80
Al15	Cascade	2,28	2,58	11,8	2,9	5071	2769	11,56
Al16	Cascade	2,31	2,57	10,3	0,2	4974	2735	11,49
Al17	Wfall.	2,28	2,66	14,2	8,3	4711	2605	10,74
Al18	Wfall.	2,11	2,65	20,4	10,3	4703	2557	9,91
Al19	Casc.	2,44	2,56	4,5	0,2	5663	2987	13,84
Al20	Casc.	2,37	2,58	8,3	1,0	5511	2952	13,05
SU01	Pool	2,52	2,65	5,2	/	5670	3063	14,26
SU02	Reed	2,31	2,68	14,0	/	5283	2834	12,19
SU03	Pool	2,53	2,66	5,1	/	5787	3070	14,63
SU04	Reed	2,34	2,69	13,0	/	5333	2859	12,48
SU05	Reed	1,80	2,71	33,5	/	3695	2037	6,65
SU06	Reed	1,77	2,71	34,7	/	3879	2149	6,86
SU07	Pool	2,51	2,65	5,4	/	5386	2899	13,49
SU08	Reed	2,35	2,69	12,9	/	5386	2899	12,64
SU09	Reed	2,25	2,69	16,2	/	5408	2866	12,16
SU10	Reed	2,33	2,65	12,1	/	5364	2863	12,50
SU11	Reed	2,17	2,70	19,5	/	4942	2685	10,73
SU12	Reed	2,24	2,70	16,9	/	5217	2834	11,71
SU13	Pool	2,56	2,66	3,8	/	5809	3091	14,89
SU14	Reed	2,20	2,68	17,8	/	4974	2714	10,95
SU15	Reed	2,33	2,68	13,3	/	5590	2976	13,01
SU16	Pool	2,41	2,70	10,6	/	5335	2867	12,87
SU17	Pool	2,32	2,70	14,0	/	5104	2759	11,86
SU18	Pool	2,53	2,65	4,4	/	5739	3027	14,55
SU19	Pool	2,53	2,67	5,2	/	5668	2996	14,36
SU20	Pook	2,52	2,69	6,5	/	5617	2933	14,15
SU21	Pool	2,57	2,67	3,8	/	5580	3107	14,33
BU01	Pool	2,32	2,67	13,2	0,1	5320	2883	12,33
BU02	Pool	2,33	2,64	12,0	0,2	5409	2892	12,59
BU03	Pool	2,33	2,67	12,7	0,1	5738	3010	13,39
BU04	Pool	2,41	2,65	9,0	0,1	5569	2961	13,42
BU05	Casc.	2,39	2,66	10,1	0,1	5470	2899	13,07
BU06	Casc.	2,40	2,66	9,9	0,1	5345	2908	12,83
BU07	Casc.	2,43	2,66	8,4	0,1	5437	2942	13,22
BU09	Casc.	2,37	2,66	10,9	0,1	5195	2840	12,33
BU10	Casc.	2,26	2,66	15,0	0,8	5507	2917	12,47
BU11	Reed	2,19	2,68	18,1	7,0	5363	2834	11,75
BU12	Reed	2,29	2,66	14,1	412,1	6097	3140	13,94
BU13	Reed	2,43	2,66	8,4	0,5	5542	2982	13,49
BU14	Reed	2,12	2,66	20,3	19,2	5305	2840	11,26
BU15	Reed	2,38	2,65	10,0	0,4	5460	2897	13,01
BU16	Reed	2,32	2,67	12,8	3,4	5260	2816	12,23
BU18	Marl	2,46	2,66	7,5	3,1	5881	3020	14,44
BU19	Reed	2,08	2,68	22,4	18000,0	5304	2792	11,02
BU20	Marl	2,43	2,65	8,2	23,8	5600	2980	13,63
BU21	Marl	2,49	2,65	5,9	/	5896	2941	14,69
BU23	Reed	1,97	2,68	26,4	/	5292	2668	10,44

[a]Dry density (ρ_d), grain density (ρ_g), porosity (ø), p-wave velocity (V_p), s-wave velocity (V_s), Klinkenberg permeability (Kl. perm), Acoustic Impedance (A.I.), Cascade (Casc), Waterfall (Wfall) and not determined (ND).

The retrograde path of most samples, however, is characterised by a slower velocity decrease with pressure than expected from the prograde path (figure 7). Compressional-wave velocities at the end of the analysis will be slightly higher than at starting conditions. The deformation inflicted during the prograde path is in this case non-elastic. Here, instable micro-fractures and pores likely remain closed after applying maximum pressures of 40MPa. The edges of the samples are in some cases slightly affected. However, none of the retrograde paths show faster velocity decrease with pressure than observed in their prograde path, indicating that none of the samples disintegrated during the analyses.

Both compressional- and shear-wave velocities were plotted against the Helium porosities (figure 8). Despite the fact that samples were collected from three different locations, they all define one trend. The acoustic velocities are dependent on the bulk densities (Kearey et al., 2002). Since there is hardly any change in the grain density of the samples, the bulk density is almost solely dependent on the porosity. Therefore, compressional-wave, shear-wave velocity and porosity are expected to be inversely proportional. Both V_p and V_s show an increasing trend with decreasing porosity. Their correlation coefficients are 0.70 and 0.78, respectively.

The dataset can be subdivided into three groups based on differences in petrographical characteristics. For each group, the corresponding porosity and acoustic velocity ranges are delineated.

The **first group** is populated by compact and dense, laminated continental carbonates. These compact carbonates are comprised of micrite with occasionally patchy distributed reworked continental carbonate clasts. The porosity in these samples is restricted to interparticle microporosity. Laminated continental carbonates contain (sub-) horizontal alternating micritic and sparitic layers or are composed of interlocking and sloping dendritic crusts. Peloids are important

building components for continental carbonates of group one. Interpeloidal porosity often follows lamination on macroscale and because of their intergranular, in this case interpeloidal, nature, they are referred to as pseudo-fenestrae (Flügel 2010). These pores can be macroscopically recognised by their grainy aspect. Real fenestral porosity has also been observed, resulting from a combination of the decay of algal mats, plant fragments, organic matter in general and possible air entrapment (Claes et al, Submitted). Interlaminae porosity is particularly associated with dendritic crusts and occurs below these crusts. It is likely the result of encrustation of algae and/or bryophytes, or possibly other organic matter and their subsequent decay. Furthermore, the desiccation of the layers can cause shrinkage and together with the former, create shelter porosity. The above-mentioned porosity types result in relatively low total porosity of the continental carbonate samples in group 1 (2-9%). Associated V_p wave velocities vary between 5386 and 5896m/s. Specimens from the sub-horizontal and cascade facies dominate this group.

The **second group** is associated with a strong increase of plant (macrophyte, bryophyte) moulds, relict-algae content and possibly associated former microbial activity. Mouldic porosity, associated to calcite encrustation and subsequent decay of the organic matter, but also vuggy porosity and micro-framework porosity in between dendrites, are the reason for a strong increase in porosity (9 - 23%) when compared to the first group. Compressional-wave velocity ranges from 4703 – 5738 m/s. The reed facies, with abundant reed-mouldic pores, is an important contributor to this group. However, mouldic and vuggy pores also appear in the cascade and waterfall facies and vugs are to a lesser extent even found in the sub-horizontal facies. Depending on the percentage of vuggy and mouldic pores, a gradual transition exist between group 1 and group 2 samples.

In the **third group** the porosity is very high, up to 35%. Such high porosities in continental carbonates are associated with framework porosity, formed between the complex network of interfingering overcrusted former plants (bryo- and macrophyte) and other forms of organic matter. Framework

porosity is most commonly observed in the waterfall facies. Another way to achieve such high porosities is through the initiation of diagenetic processes (dissolution, pedogenesis, etc.). Samples SU05 and SU06 are strongly affected by secondary alterations and have a more friable appearance. Body wave velocities for samples with porosities above 25% vary between 3695 and 4267m/s.

Within the three respective groups, samples can be found that exhibit similar porosities, but different P-wave velocities. For example sample AL18 has a porosity of 20.2% and a V_p of 4703m/s, while AL09 has a porosity that is very similar, 19.7%, but a V_p of 5253m/s. Samples BU02 and AL08 also exhibit similar porosities, 12 and 12.9%, but different V_p values, 5409 and 5628m/s, respectively. Three samples from Budakalász (group 2: BU12, BU19 and group 3: Bu23) have higher velocities than expected based on their total porosities and were subjected to a petrographical study. All three samples show an extensive cementation with sparitic, bladed crystals. The cementation causes a colour change from white-grey to orange-brown. Two group 1 specimens (SU13 and SU18) are affected by a similar degree of cementation. However, these samples do not show a surplus in velocity and a deviation from the acoustic velocity-porosity trend line.

Compressional-wave velocities for the continental carbonates are plotted along the popular WTA (Wyllie Time-Average) and RHG (Raymer-Hunt-Gardner) porosity-to-velocity transforms (figure 9). The transforms state that the total transit time is given by the sum of the transit times of the acoustic wave in the minerals and in the pore fluids (Mavko et al., 2009; Verwer et al., 2008). The WTA and RHG transforms were modelled for pure calcite compositions, with water as pore fluid. Gassmann's fluid-substitution equation was applied to predict the water saturated bulk modulus of the dry continental carbonate samples and was used as input to calculate water saturated compressional-wave velocities.

Saturated V_p values are higher than for the dry samples (7.5% on average, with a maximal surplus in velocity of 747m/s). The measured velocities plot higher than predicted by the WTA and RHG equations. This is in agreement with earlier studies (Anselmetti & Eberli, 1993; Verwer et al., 2008), indicating that the WTA and RHG transforms predict averages for all sedimentary rock types, but require modifications towards higher velocities to predict reliable velocity-porosity couples in continental carbonates.

The elastic moduli of the samples (bulk, shear and Young's moduli, the Poisson's ratio, Lame constant and the acoustic impedance) can be calculated from the measured data. The Poisson's ratio is an elastic constant and a measure of the material compressibility perpendicular to the applied stress field. The ratio, used in seismic surveying as a diagnostic lithology indicator (Kearey et al., 2002), ranges from 0.28 to 0.33 (with a mean value of 0.3). These results are typical for carbonate rocks, which always yield a Poisson's ratio around 0.3, compared to 0.2 for sandstones, above 0.3 for shales and 0.4 for coal lithologies (Schlumberger, 2013). The acoustic (or seismic) impedance of the medium in which body waves are travelling, is the product of the P-wave velocity and bulk density of the sample. Acoustic impedance differences will influence the reflection coefficient of the rocks. The observed range in P-wave velocities and dry bulk densities results in acoustic impedance contrasts, with values between 6.7 and 14.9 10^6 Ns/m³. The acoustic impedance and porosity (figure 10) show an even better inversed correlation (0.91) than observed for V_p and porosity (0.70).

4.5. Computer Tomography (µCT)

Ten representative samples were scanned with µCT and analysed to determine the volume percentages of the existing pore types. The results of the pore type calculations are given in table 2. Thin section petrography learned that interparticle microporosity, fenestral porosity and interpeloidal porosity have flattened to equidimensional shapes (plate-, blade- and cube-like pores), while reed and bryophyte mouldic porosity have a cylindrical, strongly elongated shape. Rod- to cuboid-like pore shapes best represent the plant-mouldic pores. The pore morphology of vugs is

irregular and variable. Specimens where the sum of rod and cuboid pores exceeds 50vol% are classified as plant-mouldic porosity dominated. Three scanned samples out of 10 fulfil this criterion, i.e. AL08, AL09 and BU11. They contain 85 vol%, 89 vol% and 58 vol% rod- and cuboid-like pores, respectively.

Table 2. CT based pore type calculations

Sample number	Calculated pore shapes and their respective volumes (vol%)				
	Rod	Blade	Plate	Cube	Cuboid
AL08	35,88	3,84	5,48	5,2	49,53
AL09	2,58	1,05	3,13	6,72	86,49
AL13	9,85	2,56	30,24	34,13	23,36
AL18	23,45	49,85	7,02	3,99	15,63
AL19	10,74	20,73	24,14	14,42	29,91
BU01	3,69	4,4	30,11	21,72	39,99
BU06	5,96	4,75	43,48	15,84	29,88
BU11	31,94	2,84	9,84	28,82	26,55
BU20	11,71	2,63	4,97	68,14	12,52
SU18	7,42	4,42	64,47	9,94	13,71

In the porosity – acoustic velocity plot (figure 11) these CT scanned samples, dominated by plant-mouldic porosity, plot above the inversed exponential trend line. Other samples (AL13, AL18, AL19, BU01, BU06, BU20 and SU18) plot close to or below the trend line. The amount of plant-mouldic pores is strongly reduced in these samples, resulting in volume percentages for blade, plate and cube-like pores equal to or larger than 50vol%.

Micro-focus CT scans of sample AL09 (porosity: 19.7%, V_p: 5253m/s) and AL18 (porosity: 20.2%, V_p: 4703) revealed that their pore networks are significantly different. The 2D µCT slices show a dominance of oval shaped pores (average diameter of a few millimetres) in sample AL09 (figure 12A), compared to a dominance of more uniformly distributed oblate (micro)pores in AL18, with a diameter of several 10s to 100s of micrometers (figure 12B). A shell fragment can also be observed in the latter.

AL09 is characterised by 86 vol% cuboid-like pores. This can be observed in the volume rendered and labelled pore network (figure 12C), where relict plant rods running through the entire sample can be

readily recognised. The oval shaped pores in the 2D slices are transects perpendicular to the length axis of the rods. In sample AL18, blade-, cubic- and plate-like pores dominate the network (figure 12D). The smaller pore sizes in the latter sample require a larger quantity of pore objects to achieve a similar porosity as for the rod shape dominated sample. Hence, the porosity distribution is significantly different for both samples, patchy versus uniform respectively, implying that body waves will propagate in a different manner (Anselmetti & Eberli, 1993; Brigaud et al., 2010; Verwer et al., 2008).

5. Discussion

The continental carbonates of this study exhibit large-scale ranges for both porosity and permeability. This is in line with expectations, given the petrographically observed (both on micro- and macroscale) heterogeneity of these limestones. The continental carbonates underwent a shallow burial history. The V_p/V_s ratio for all the samples varies between 1.8 and 2, which are values corresponding to indurated carbonates (Anselmetti & Eberli, 1993). This strongly suggests that artificial compaction was limited during the ultrasonic velocity analyses and that the continental carbonate samples were strong enough to sustain the applied shear stresses. This illustrates that continental carbonates, even under limited burial conditions, can develop rigid rock frames that allows them, to a certain degree, to withstand compaction. Both V_p and V_s are reversely correlated with the sample porosity. The permeability is dependent on the porosity and connectivity between the individual pore bodies. However, no clear poro-perm correlation was found for these carbonates that exhibit complex texture and property distributions. These complexities also make it difficult to understand relationships between seismic velocity and permeability. Factors that might influence this relationship are the isotropic nature of porosity on the one hand and the anisotropic nature of permeability and acoustic velocity on the other hand. Saleh et al. (2008) found an apparent trend between shear-wave velocity and permeability in samples where velocity measurements were

perpendicular to the direction of preferential permeability. The pore network tortuosity and complex flow paths in continental carbonates, however, might ensure that this trend is not observed. Experimental measurements are needed to unravel the acoustic velocity – permeability relationship.

Texture specific variations can be observed along the porosity – acoustic velocity trend line for continental carbonates. The acoustic velocity dataset was subdivided into three groups, based on the petrographic characteristics of the samples. For each group, porosity and acoustic velocity ranges were delineated. The cementation of group two samples results in more rigid self-supporting rock frames in between plant-mouldic pores and framework pores. Cements generally enhance the contact between individual crystals and building components throughout the sample. It will be these well developed connections and higher rigidity that facilitate acoustic wave propagation (Anselmetti & Eberli, 1993; Verwer et al., 2008). Group 1 samples contain a primary, compact and dense fabric, which easily transmits body waves. Building constituents of Group 1 samples are better connected and the effect of the cementation is expected to be limited when compared to more porous Group 2 and Group 3 samples.

Some continental carbonate samples with similar porosity values have very distinct body wave propagation velocities. In siliciclastic rocks, this range would be explained by differences in sediment composition and associated mineralogy. The continental carbonates in this study, however, consist almost exclusively of calcite and even aragonite was not retrieved in the XRD analysis. This means that either aragonite never precipitated in the study area or that the pre-existing aragonite crystals underwent a complete transformation to calcite. The mono-mineralic nature of these continental carbonates suggests that factors, other than mineralogy, might be responsible for the differences in body wave propagation velocities. Most likely fabric and texture of the continental carbonates play an important role in the propagation speed of P- and S-waves (Anselmetti & Eberli, 1993; Verwer et al., 2008). Although diagenetic modifications hardly affected these samples and a strong porosity

control on the compressional- and shear-wave velocities exists, pore morphologies and distributions may be important features explaining these specific discrepancies.

µCT showed that the pore networks of sample AL09 and AL18, with similar porosities but distinct P-wave velocities, are significantly different. A compressional wave travelling through a sample will encounter pores. When the pores are uniformly distributed throughout the sample, more pore objects will be encountered by the wave, resulting in a scattered wave front. In samples where plant-mouldic pores predominate (AL09), a rigid, micritic, self-supporting framework surrounds the moulds with sparite cement rims. The rigid frame permits fast travel times for the wave front, with limited scatter. This framework-travelling time correlation explains why sample AL09, which has a similar porosity as sample AL18, possesses velocities that are higher than expected based on their total porosities (Anselmetti & Eberli, 1993). The observed difference in pore sizes, quantity of pore objects, shapes and their distribution results in the observed body-wave velocity discrepancies (Anselmetti & Eberli, 1993; Brigaud et al., 2010; Verwer et al., 2008).

The influence of pore types on the acoustic-wave velocity is also reported for marine carbonates. Dense, low porous samples generally plot close to the velocity known of pure calcites (6260-6640m/s, (Mavko et al., 2009)) similar velocities were reported for continental carbonate samples in group 1 (figure 9 with ≤ 9% porosity). Fabric selective porosity types, such as interparticle and intercrystalline porosity tend to plot in the lower velocity area (Eberli et al., 2003). However, Weger et al. (2009) showed for various case studies that these pore types may plot over the entire velocity range. The velocity increase associated with mouldic and vuggy porosity and the decrease associated with microporosity as shown by various authors (Anselmetti & Eberli, 1993; Eberli et al., 2003; Fournier & Borgomano, 2007; Weger et al., 2009) agree with the findings of our study. The velocity decrease is proportional to the percentage of micropores inside the sample. Plant-mouldic pores plot at higher velocities than those of micro- and intercrystalline pore types. In addition, Weger et al.

(2009) reported that large pores with simple pore structures, as for example the rod-like plant-mouldic pores, generally result in higher acoustic velocities. Framework porosity in this study is, in contrast to marine carbonates, associated with a lowering in velocity when compared to the general trend. The elastic rigidity of hollow encrusted reed stems, the framework builders in continental carbonates, is lower than the rigidity of corals and bryozoans of a reefal growth framework (Eberli et al., 2003; Weger et al., 2009). This lower rigidity results in slower wave propagation.

The direct comparison between acoustic velocities in continental carbonates, the trend line for compressional-wave velocities based on our own data, and those in marine carbonates of Weger et al. (2009) and of Anselmetti & Eberli (1993) shows remarkable differences. Figure 13 shows trend lines for compressional-wave velocities, with their respective porosity range for aforementioned datasets.

The blue trend line (figure 13) is based on 120 marine carbonate plugs (Weger et al., 2009). The samples originate from two drowned cool-subtropical platforms on the Marion Plateau (Miocene age) in Australia (Baechle et al., 2004), from the Shu'aiba Formation in the Middle East (Aptian age) and from an isolated carbonate platform (Miocene age) in Southeast Asia. The specimens are limestones, containing minor amounts of dolomite and less than 2% non-carbonate minerals. The porosity for these samples ranges between 8 and 45%. An inverse exponential correlation illustrates the relationship between sample porosity and compressional-wave velocities.

The red trend line (figure 13) represents petrophysical data of Anselmetti & Eberli (1993) and includes 190 marine carbonates. The samples originate from Montagna della Maiella in Abruzzi, Italy and from cores from the Great Bahama Bank. These sediments are calcite dominated and have a porosity range of 0 to 58%.

The purple trend line (figure 13) is derived from Eberli et al. (2003), which are measurements of pure carbonate rocks from the Great Bahama Bank, ODP Site 1003, and Hole Unda. These sediments exhibit porosities from 0 to 55%.

Despite the differences in porosity and mineralogy (dominantly calcite, but also dolomite and aragonite) in the marine carbonates, similar porosity-velocity paths can be observed. The blue (Weger et al, 2009) trend line deviates slightly from the purple (Eberli et al., 2003) and red (Anselmetti & Eberli, 1993) trend lines. The surplus in velocity (especially visible at lower porosities) is possibly related to the number of vug dominated specimens in the 10-15% porosity range. Together with the reduced microporosity in this area of the porosity-velocity cross plot, this can result in a shift of the trend line towards higher velocities. Generally it seems that pure carbonate samples with similar porosities, but from different locations in the marine realm, come up with similar compressional-wave velocities.

The trend line for the continental carbonates, however, defines a different path. In the direction of ascending porosity, the trend lines for marine and continental carbonates diverge and V_p values in continental carbonates become gradually higher than V_p values in marine carbonates with similar porosities. The continental carbonate trend line exhibits a generally less steep slope with an inverse exponential relation over the entire porosity-velocity area.

Continental carbonates thus produce porosity - acoustic velocity equations that significantly differ from those known from pure marine carbonates. Apparently does the nature of the marine and continental limestones play a decisive role in the velocity differences. Continental carbonates on the one hand are predominantly precipitates that form an in situ rigid rock frame (often called framestone, (Ford & Pedley, 1996; Özkul et al., 2010; Pedley, 2009)). Even at the surface or after minor burial they have considerable compressive and shear strength, as indicated by the high

pressure ultrasonic measurements. Marine carbonates on the other hand consist of (cemented) transported sediments, resulting in a rock frame that permits slower wave propagation when compared to the continental limestones. Other differences that might influence wave velocities are the grain sizes and uniformity of the grain size distribution in marine carbonates versus crystal sizes (micrite and sparite) in continental carbonates (Samsuri & Herianto, 2005; Wichtmann & Triantafyllidis, 2010).

6. Conclusion

The continental carbonates in this study were subjected to a multi-technique approach (porosity, permeability, acoustic velocity and computer tomography analyses) and provide a more in depth understanding of these carbonates and their petrophysical properties.

Quaternary continental carbonates from quarries in Denizli (Turkey) and from Süttő and Budakalász (Hungary) are petrophysically heterogenous with porosities varying from 2.8 to 34.7% and permeabilities ranging between 0.05 and 18.000mD. The heterogeneity results from a complex primary fabric, texture and large scale pore type variability. The continental carbonates are predominantly mono-mineralic, almost purely calcite. Despite the remarkably wide range of velocities in continental carbonates (over 2400m/s for V_p and 1100m/s for V_s), the acoustic velocities of the samples that originate from three different locations, define one trend that clearly exhibits an inverse relation with sample porosity. The inverse relation is expected since the propagation of ultrasonic wave fronts is impeded in porous specimen. Shear wave velocities in a sample are approximately 50 - 55% of the compressional wave velocities of the same sample, yielding Vp/Vs ratios of 1.8-2. These ratios are typical for all carbonates. The compressive strength of the rock frame ensures that porosity can be retained during burial and results in high reservoir potentials for these continental carbonates.

Based on petrographical characteristics, specimens could be subdivided into three groups with predictable ranges for porosity and body wave velocity. The first group shows low porosity (2 - 9%), compact, dense and layered continental carbonates, with V_p wave velocities of 5386 to 5896m/s. The pore network of samples in this group is mainly made up of interparticle, interpeloidal, fenestral and interlayer porosity. It is expected that the dense nature of these samples and the associated low porosities provide good passages for the wave fronts, hence the relatively high wave velocities. Samples in the second group are associated with mouldic and vuggy porosity (9 - 23%). The increase in porosity partly blocks the propagation of the wave fronts, yielding velocities of 4703 to 5738m/s. In the third group diagenetic alterations, pedogenesis and primary framework porosity results in porosities exceeding 25%. Such high porosities impede the propagation of wave fronts even further. The compressional velocity is thus lowered to values of 3695 – 4267 m/s.

The petrophysical analysis made clear that not the mineralogy, but both primary fabric (especially the overall porosity, the specific pore types), and the degree of cementation influence the velocity of ultrasonic waves in continental carbonate samples. Cementation has more effect on wave propagation in the highly porous samples (≥ 15% porosity). This is illustrated by their positive departure from the best-fit curve. Low porosity samples have a dense nature, with interlocking crystals and touching particles in the sample matrix. Therefore, the surplus in wave velocity, provided by cements that connect different rock fabric components, will be limited. Not only cemented samples, but also patchy distributed plant-mouldic porosity is often associated with a positive departure from the acoustic velocity-porosity trend line. In this case, the rigid frame in between the moulds provides high velocity pathways for the wave fronts.

Acoustic impedance data fall in between 6.7 and 14.9 (10^6 Ns/m³). The range is caused by the variations in velocities and dry bulk densities. Seismic sections in mono-mineralic carbonate systems

can thus contain seismic reflectors that are not caused by non-carbonate intercalations, but relate to geobody boundaries, in which the seismic expression is function of porosity and pore types. The dependence of the acoustic impedance on the porosity is illustrated by the strong correlation between both parameters. The comparison of acoustic velocities in continental carbonate rocks with those in pure, marine carbonates revealed that the continental carbonate best fit curve for porosity versus compressional-wave velocity follows a different trajectory for a similar porosity domain. Body wave velocities in continental carbonates show a slower decrease with increasing porosity. This study provides insight in the petrophysical properties, i.e. porosity, permeability and acoustic velocities of continental carbonates and is of high importance for acoustic and reservoir modeling in subsurface continental carbonate reservoirs (Buckley et al.,2013).

7. Acknowledgements

My thanks goes to the owners and managers of the Alimoğlu, Új Haraszti and Budakalász quarries, for providing us with the opportunity to work in actively excavated quarries.

I am grateful to Mr. Tuur Smekens and Mr. Mathieu Degros for their help during the field work in Hungary and for doing their part in the acoustic properties analysis.

I would like to thank Herman Nijs, for the preparation of the thin sections and his aid with practical matters during the sample preparation processes.

The authors would like to acknowledge the Hercules foundation (Flanders) for founding the micro- and nano-CT for the hierarchical analysis of materials project.

Soete J. is funded by a Ph.D grant from ‘agentschap voor Innovatie door Wetenschap en Technologie’ (IWT), Flanders, Belgium.

8. References

Alonso-Zarza, A.M., Tanner, L.H., 2010. Carbonates in continental settings, Facies, environments and processes, Elsevier.

Anselmetti, F.S., Eberli, G.P., 1993. Controls on sonic velocity in carbonates. *Pure and Applied Geophysics PAGEOPH* 141(2-4), 287–323.

Aslanian, D., Moulin, M., Olivet, J.-L., Unternehr, P., Matias, L., Bache, F., Rabineau, M., Nouzé, H., Klingelheofer, F., Contrucci, I., Labails, C., 2009. Brazilian and African passive margins of the Central Segment of the South Atlantic Ocean: Kinematic constraints. *Tectonophysics* 468(1-4), 98–112.

Bakacsi, Z.S., Mindszenty, A., Hertelendi, E., 1994. Lacustrine-palustrine facies from the Pleistocene Carbonate lake of Süttő (Hungary). In: IAS 15th Reg. Meeting, Ischia, Italy, Abstract, 41–42.

Baechle, G.T., Weger, R., Eberli, G.P. and Massaferro, J.L., 2004. The role of macroporosity and microporosity in constraining uncertainties and in relating velocity to permeability in carbonate rocks. *Society of Exploration Geophysicists*, Expanded Abstracts 23.

Biot, M.A., 1956. Theory of Propagation of Elastic Waves in a Fluid-saturated Porous Solid, I. Low Frequency Range, II. Higher Frequency Range, *J. Acoust. Soc. Am*. 28, 168-191.

Bozkurt, C., Bozkurt, E., 2009. Pattern of normal faulting in the Gediz Graben, SW Turkey. T*ectonophysics* 473(1-2), 234–260.

Braaksma, H., Kenter, J.A.M., Proust, J.N., Dijkmans, V., Van Hoek, T., Mahieux, G., Drijkoningen, G.G., 2003. Case History Controls on acoustic properties of Upper Jurassic siliciclastic rocks (Boulonnais, northern France). *Geophysics* 68(1), 58–69.

Brigaud, B., Vincent, B., Durlet, C., Deconinck, J.-F., Blanc, P., Trouiller, A., 2010. Acoustic Properties of Ancient Shallow-Marine Carbonates: Effects of Depositional Environments and Diagenetic Processes (Middle Jurassic, Paris Basin, France). *Journal of Sedimentary Research* 80(9), 791–807.

Buckley, J.P., Elders, C., Mann, J., 2013. Carbonate Buildups in the Santos Basin, Offshore Brazil. Programme and Abstract Volume: Microbial Carbonates in Space and Time: Implications for Global Exploration and Production. *The Geological Society,* London, 37-39.

Claes, H., Soete, J., El Desouky, H.A., Van Noten, K., Özkul, M., Swennen, R., Submitted. Diagenesis and geochemistry of the travertine quarries Ece & Faber, Ballık area, Denizli, South-West Turkey. *Sedimentology*.

Claes, S., Soete, J., Claes, H., Swennen, R., 2013. 3D visualization and quantification of the porosity network in travertine rocks. *The Geological Society,* London, 79-81.

Dewit, J., Huysmans, M., Muchez, P., Hunt, D.W., Thurmond, J.B., Verges, J., Saura, E., Fernandez, N., Romaire, I., Esestime, P., Swennen, R., 2012. Reservoir characteristics of fault-controlled hydrothermal dolomite bodies: Ramales Platform case study. *Geological Society, London, Special Publications* 370(1), 83–109.

Dolton, G., 2006. Pannonian Basin Province, Central Europe (Province 4808)-Petroleum Geology, Total Petroleum Systems and Petroleum Resource Assessment. *USGS*, (Province 4808).

Eberli, G., Baechle, G., Anselmetti, F., Incze, M., 2003. Factors controlling elastic properties in carbonate sediments and rocks. *The Leading Edge*, 654 – 660.

El Desouky, H.A., Soete, J., Claes, H., Özkul, M., Vanhaecke, F., Swennen, R., submitted. Genesis of the Ballık travertines, Denizli Basin, Western Turkey: Evidence from fluid inclusions and isotope geochemistry. *Sedimentology*.

Flügel, E., 2010. Microfacies of carbonate rocks. Second edition, Springer-Verlag.

Ford, T.D., Pedley, H.M., 1996. A review of tufa and travertine deposits of the world. *Earth-Science Reviews* 41(3-4), 117–175.

Fouke, B.W., 2011. Hot-spring Systems Geobiology: abiotic and biotic influences on travertine formation at Mammoth Hot Springs, Yellowstone National Park, USA. *Sedimentology* 58(1), 170–219.

Fournier, F., Borgomano, J., 2007. Geological significance of seismic reflections and imaging of the reservoir architecture in the Malampaya gas field (Philippines). *AAPG Bulletin* 91(2), 235–258.

García-del-Cura, M.Á., Benavente, D., Martínez-Martínez, J., Cueto, N., 2012. Sedimentary structures and physical properties of travertine and carbonate tufa building stone. *Construction and Building Materials* 28(1), 456–467.

Gassmann, F., 1951. Elastic Waves through a Packing of Spheres, *Geophysics* 16, 673 685.

Goldscheider, N., Mádl-Szőnyi, J., Erőss, A., Schill, E., 2010. Review: Thermal water resources in carbonate rock aquifers. *Hydrogeology Journal* 18(6), 1303–1318.

Gundogan, I., Helvaci, C., Sozbilir, H., 2008. Gypsiferous carbonates at Honaz Dağı (Denizli): First documentation of Triassic gypsum in western Turkey and its tectonic significance. *Journal of Asian Earth Sciences* 32(1), 49–65.

Guo, L., Riding, R., 1998. Hot-spring travertine facies and sequences, Late Pleistocene, Rapolano Terme, Italy. *Sedimentology* 45(1), 163–180.

Gürer, Ö.F., Yilmaz, Y., 2002. Geology of the Ören and Surrounding Areas , SW Anatolia. *Turkish Journal of Earth Sciences* 11, 1–13.

Haas, J., 2012. Influence of global, regional, and local factors on the genesis of the Jurassic manganese ore formation in the Transdanubian Range, Hungary. *Ore Geology Reviews* 47, 77–86.

Kearey, P., Brooks, M., Hill, I., 2002. An introduction to geophysical exploration, Blackwell publishing

Kele, S., Vaselli, O., Szabó, C., Minissale, A., 2003. Stable isotope geochemistry of Pleistocene travertine from Budakalász (Buda Mts., Hungary). *Acta Geologica Hungarica* 46(2), 161–171.

Kele, S., Özkul, M., Fórizs, I., Gökgöz, A., Baykara, M.O., Alçiçek, M.C., Németh, T., 2011. Stable isotope geochemical study of Pamukkale travertines: New evidences of low-temperature non-equilibrium calcite-water fractionation. *Sedimentary Geology* 238(1-2), 191–212.

Kenter, J.A.M., Fouke, B.W., Reinders, M., 1997. Effects of differential cementation on the sonic velocities of Upper Cretaceous skeletal grainstones (southeastern Netherlands). *Journal of Sedimentary Research* 67(1), 178–185.

Lapponi, F., Casini, G., Sharp, I., Blendinger, W., Fernandez, N., Romaire, I., Hunt, D., 2011. From outcrop to 3D modelling: a case study of a dolomitized carbonate reservoir, Zagros Mountains, Iran. *Petroleum Geoscience* 17(3), 283–307.

Mavko, G., Mukerji, T., Dvorkin, J., 2009. The Rock Physics Handbook, Second ed. Cambridge.

Nador, A., 1993. Paleokarsts and long-term karst evolution of the Buda Mountains, Hungary. *Bulletin de la Societe Geographique de Liège*, 139–143.

Van Noten, K., Claes, H., Soete, J., Foubert, A., Özkul, M., Swennen, R., 2013. Fracture networks and strike–slip deformation along reactivated normal faults in Quaternary travertine deposits, Denizli Basin, western Turkey. *Tectonophysics* 588, 154–170.

Nurmi, R., Standen, E., 1997. Carbonates, the inside story. *Middle East Well Evaluation Review* 18, 28–41.

Özkul, M., Varol, B., Alçiçek, M.C., 2002. Depositional environments and petrography of denïzlï travertines. *Mineral Res. Expl. Bul.* 125, 13–29.

Özkul, M., Gökgöz, A., HorvatincIc, N., 2010. Depositional properties and geochemistry of Holocene perched springline tufa deposits and associated spring waters: a case study from the Denizli Province, Western Turkey. *Geological Society, London, Special Publications* 336(1), 245–262.

Özkul, M., Kele, S., Gökgöz, A., Shen, C.-C., Jones, B., Baykara, M.O., Fórizs, I., Németh, T., Chang, Y.-W., Alçiçek, M.C., 2013. Comparison of the quaternary travertine sites in the Denizli extensional basin based on their depositional and geochemical data. *Sedimentary Geology* 294, 179–204.

Özkul, M., Gökgöz, A., Kele, S., Baykara, M.O., Shen, C.-C., Chang, Y.-W., Kaya, A., Hançer, M., Aratman, Cï., Akin, T., Örü, Z., 2014. Sedimentological and geochemical characteristics of a fluvial travertine: A case from the eastern Mediterranean region E. Capezzuoli, ed. *Sedimentology* 61(1), 291–318.

Pedley, H.M., Rogerson, M., 2010. Tufas and Speleothems Unravelling the Microbial and Physical Controls, Geological Society.

Pentecost, A., 2005. Travertine. Geologist association, Springer.

Saleh, M., Prasad, M., Vega, S., Sharma, R., 2008. A Study of Permeability and Velocity Anisotropy in Carbonates. The Petroleum Institute, 1–9.

Samsuri, A., Herianto, H., 2005. The effect of grain size distributions on acoutic wave velocities in porous rocks. *In: 8th. International Conference on Quality in Research (QIR)*, University Indonesia, Jakarta, Indonesia.

Sant'Anna, L.G., Riccomini, C., Rodrigues-Francisco, B.H., Sial, A.N., Carvalho, M.D., Moura, C.A. V., 2004. The Paleocene travertine system of the Itaboraí basin, Southeastern Brazil. Journal of South American Earth Sciences 18, 11–25.

Sierralta, M., Kele, S., Melcher, F., Hambach, U., Reinders, J., van Geldern, R., Frechen, M., 2010. Uranium-series dating of travertine from Süttő: Implications for reconstruction of environmental change in Hungary. Quaternary International 222(1-2), 178–193.

Sun, S., 1990. Denizli-Uşak arasının jeolojisi ve linyit olanakları (geology and lignite potential between Denizli and Uşak). Scientific report of the General Directorate of Mineral Research and Exploration of Turkey; No: 9985, Ankara, Turkey (in Turkish).

Thompson, L., Oftebro, C., 2011. Salt gets in your eyes: the geological challenges and solutions to sub-salt exploration. *Image (Rochester, N.Y.)* 29(March), 93–98.

Toumelin, E., Chen, S., Fischer, D.M., 2003. Reconciling NMR Measurements and Numerical Simulations : Assessment of Temperature and Diffusive Coupling Effects on Two-Phase Carbonate Samples 1. *Petrophysics* 44(2), 91–107.

Verwer, K., Braaksma, H., Kenter, J.A.M., 2008. Case History Acoustic properties of carbonates : Effects of rock texture and implications for fluid substitution. *Geophysics* 73(2), B51–B65.

Wang, Z., Hirsche, W.K., and Sedgwick, G., 1991. Seismic Velocities in Carbonate Rocks, *Can. Petr. Tech.* 30, 112-122.

Weger, R.J., Eberli, G.P., Baechle, G.T., Massaferro, J.L., Sun, Y.-F., 2009. Quantification of pore structure and its effect on sonic velocity and permeability in carbonates. *AAPG Bulletin* 93(10), 1297–1317.

Wichtmann, T., Triantafyllidis, T., 2010. On the influence of the grain size distribution curve on P-wave velocity, constrained elastic modulus M max and Poisson's ratio of quartz sands. *Soil Dynamics and Earthquake Engineering* 30(8), 757–766.

Bruker, 2013. DIFFRAC^{plus} EVA. Available at: http://www.bruker.com/products/x-ray-diffraction-and-elemental-analysis (Accessed: 22th August 2013).

Cartographic Research Lab University of Alabama, 2013. European Countries. Available at: http://alabamamaps.ua.edu/contemporarymaps/world/europe/ (Accessed: 4th October 2013).

Coelho Software, 2012. TOPAS-Academic V4.1. Available at: http://www.topas-academic.net/ (Accessed: 15th August 2013)

Schlumberger Limited, 2013. Oilfield glossary, the Poisson's ratio. Available at: *http://www.glossary.oilfield.slb.com/en/terms/p/poissons_ratio.aspx* (Accessed: 22th July 2013).

Figure Captions:

Figure 1: (A) Geological map of the Denizli Basin (After Sun, 1990, in Özkul et al., 2013), the rectangle indicates the study area. (B) Continental carbonate outcrop at the Alimoğlu quarry, excavation levels are approximately 5 to 6 metres in height.

Figure 2: (A) Geological setting of the Transdanubian Range, the rectangles indicate the Süttő and Budakalász quarries, respectively in the Gerecse Hills and Buda Mountains (modified after Haas, 2012). (B) Overview of the Új Haraszti quarry in Süttő, Hungary, each excavation level has a height of approximately 6 metres.

Figure 3: Pore type classification based on the ratios of the longest (L), intermediate (I) and shortest (S) pore dimensions.

Figure 4: Geobody and associated facies architecture of the continental carbonates with a simplified rendering of the dome structure observed in Turkey. (A) Sub-horizontal facies with (sub-) horizontal laminations and layer parallel porosity. (B) Reed facies with in situ plant casts or reed-mouldic porosity. (C) The sloping cascade facies. (D) Waterfall facies, characterised by framework and shelter porosity. (E) Brown-green coloured marl facies interfingerings with the continental carbonates.

Figure 5: Cross plot of sample porosities and Klinkenberg corrected permeabilities.

Figure 6: V_p versus V_p/V_s ratio. For the entire V_p range, the V_p/V_s ratio ranges between 1.8 and 2.

Figure 7: Examples of hysteresis loops. Inflicted deformation by the applied confining pressures is considered elastic in sample AL10, where the hysteresis loop is closed, but non-elastic in sample AL19, where the hysteresis loop is open.

Figure 8: V_p and V_s versus sample porosities. Exponential, inversed trends are observed. Regression lines provided. Labelled samples will be discussed in more detail in the text.

Figure 9: Porosity versus saturated compressional-wave velocities of the continental carbonate data set. Superimposed are the WTA and RHG transforms calculated for a matrix velocity (calcite, $CaCO_3$) of 6640m/s and a pore fluid velocity (H_2O) of 1500m/s.

Figure 10: Acoustic Impedance versus Ambient Helium porosity, displaying a strong, linear, inversed correlation.

Figure 11: V_p plotted against porosity for the samples analysed with computer tomography scanner. The Regression line of all sixty samples is provided. Specimens where the sum of rod and cuboid pores exceeds 50vol% are encircled.

Figure 12: Slices and volume rendered pore networks, extracted from µCT scans. 2D slices perpendicular to the long axis of (A) sample AL09 and (B) sample AL18. (C) Dominance of cuboid and rod-like pores in sample AL09. Plant casts, crosscutting the sample, are readily recognised. (D) Plate-like, cube and blade-like pores dominate in sample AL18. The portion of plant-mouldic pores is strongly reduced in this sample. The labelling, conducted on pore networks in C and D, assign connected pore bodies to the same colour code.

Figure 13: Inverse porosity-acoustic velocity trend lines for marine (red, purple and blue line) and continental (green line) carbonate lithologies. Trend lines are extrapolated (dashed lines) outside the porosity ranges.

Figure

Click here to download high resolution image

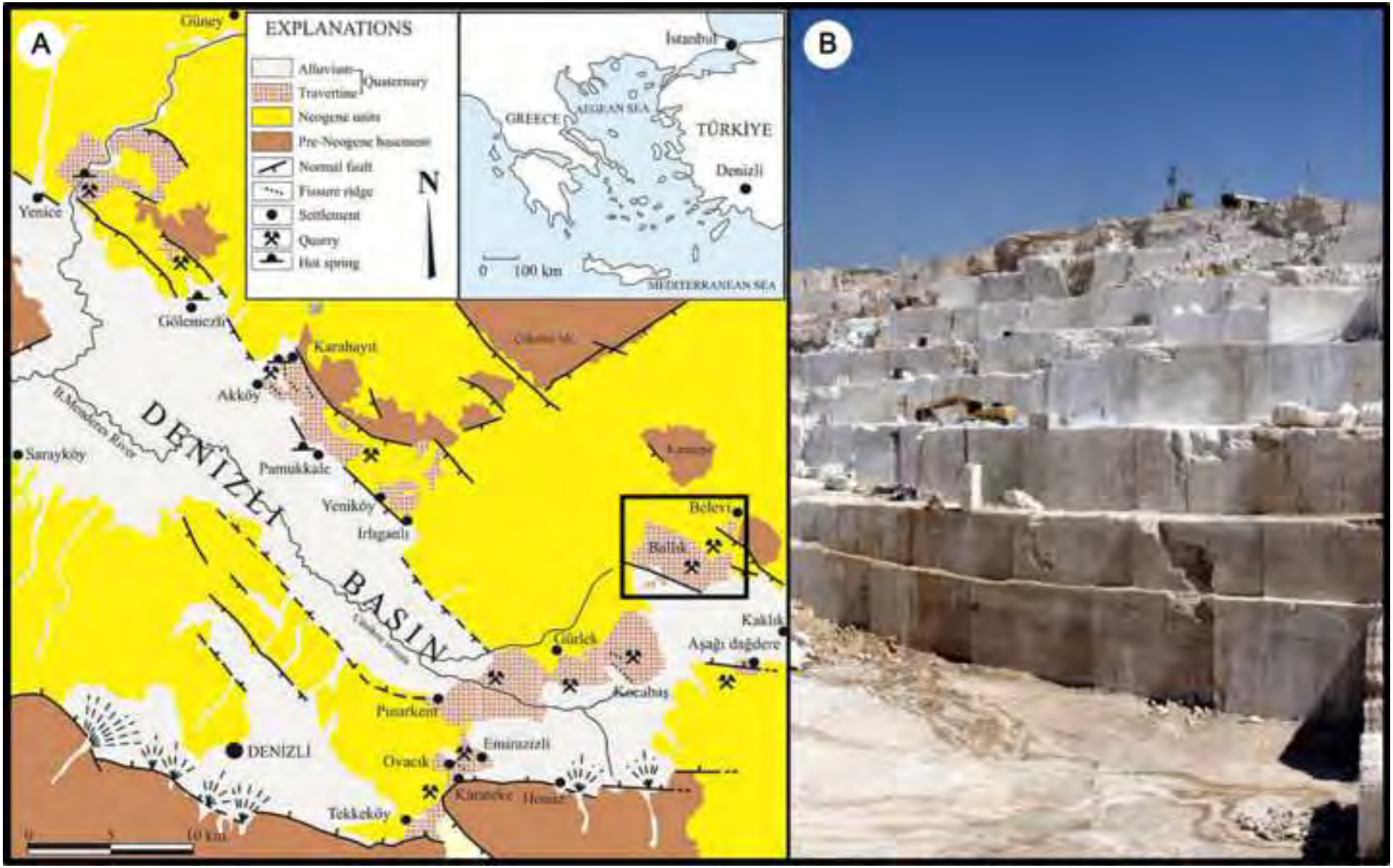

Figure

Click here to download high resolution image

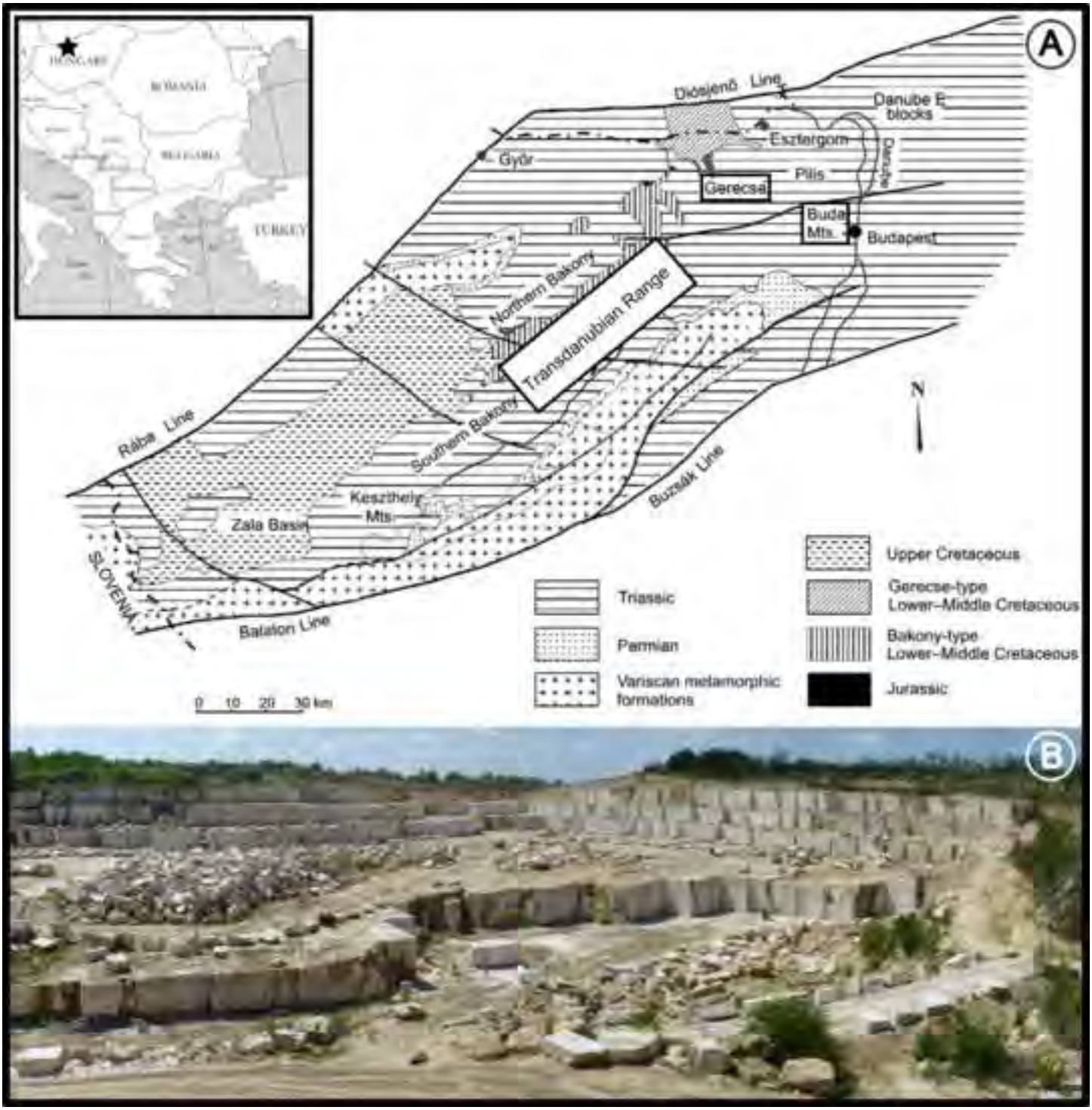

Figure

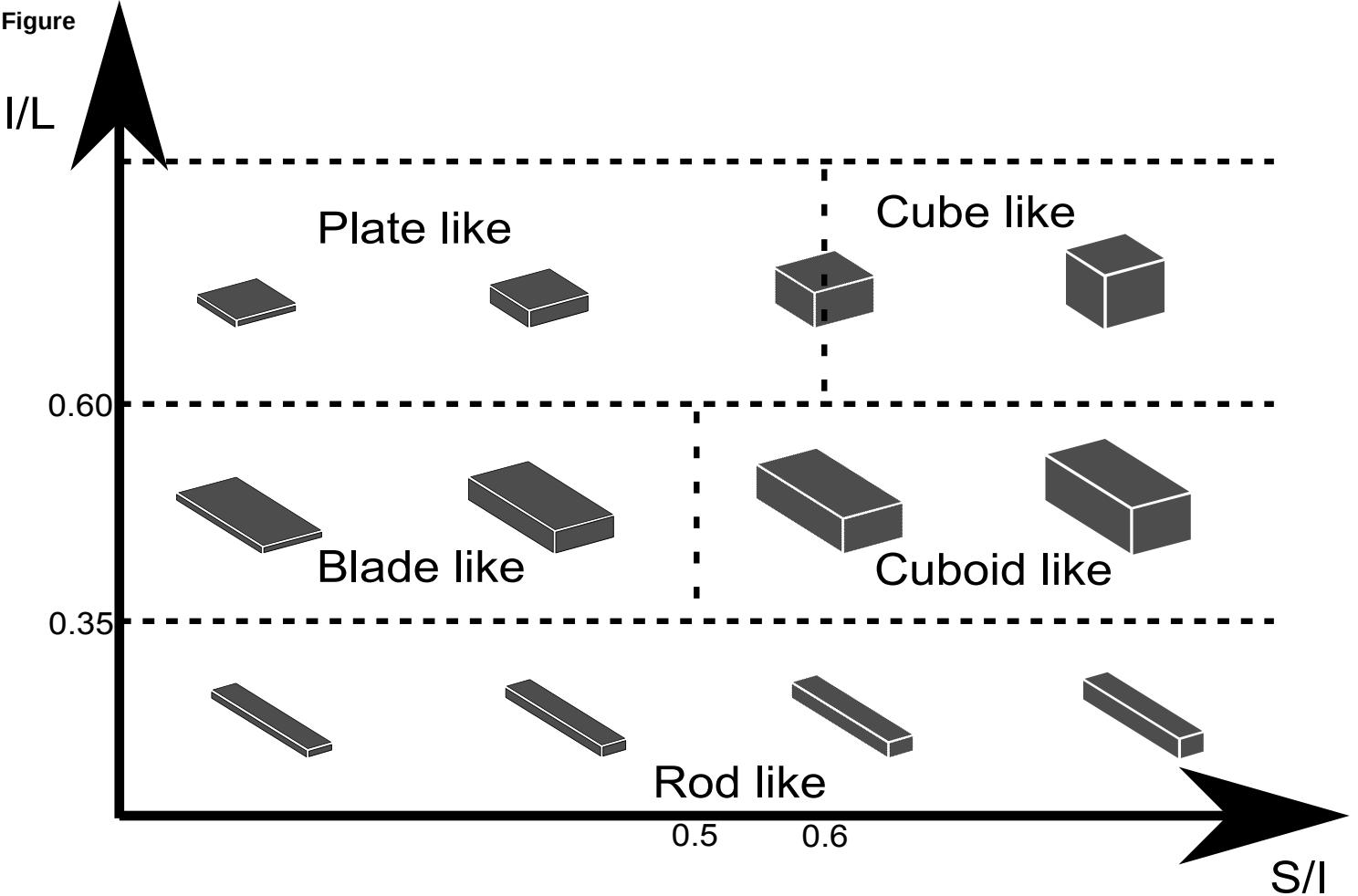
I/L
Plate like
Cube like
0.60
Blade like
Cuboid like
0.35
Rod like
0.5
0.6
S/I

Figure

Click here to download high resolution image

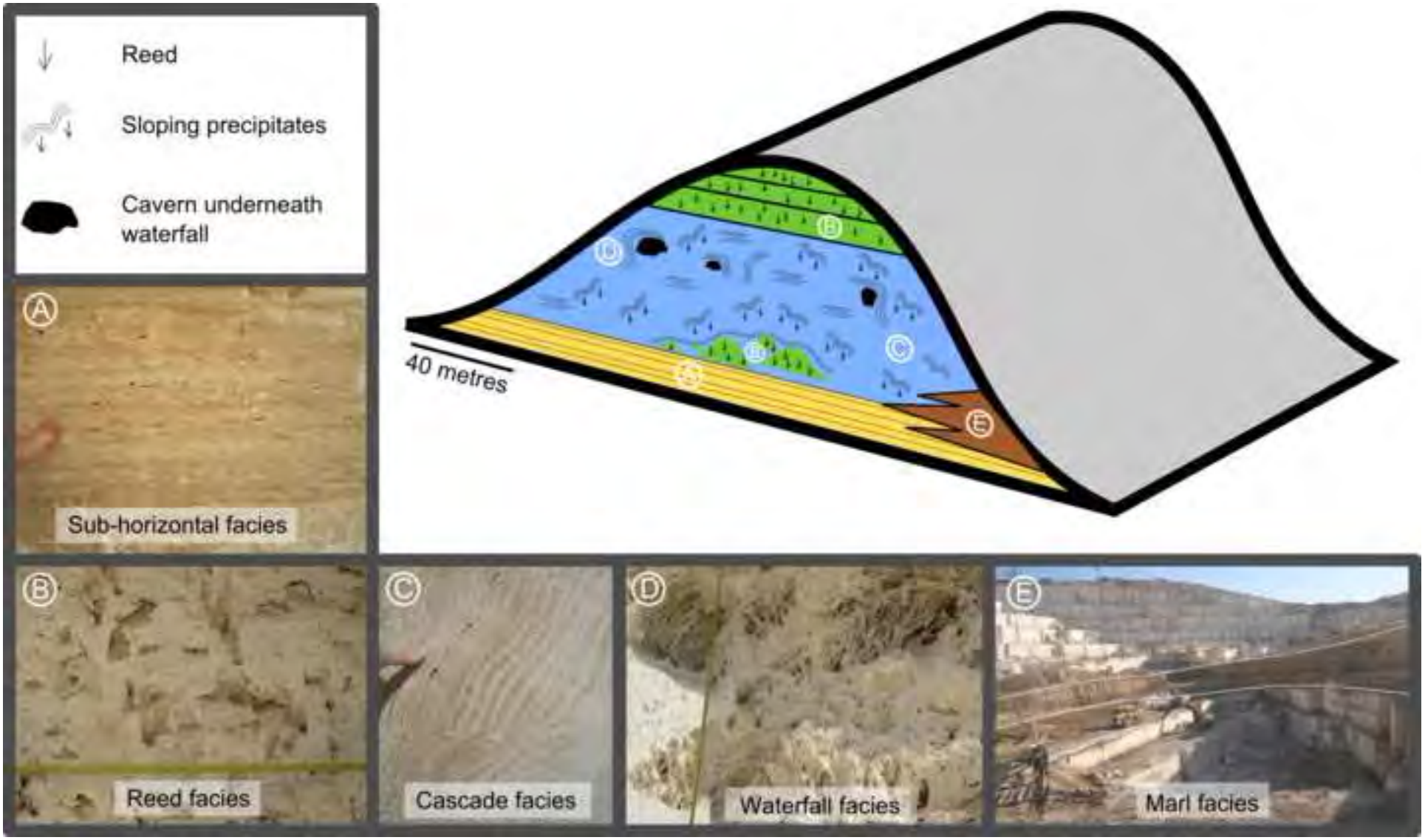

Figure

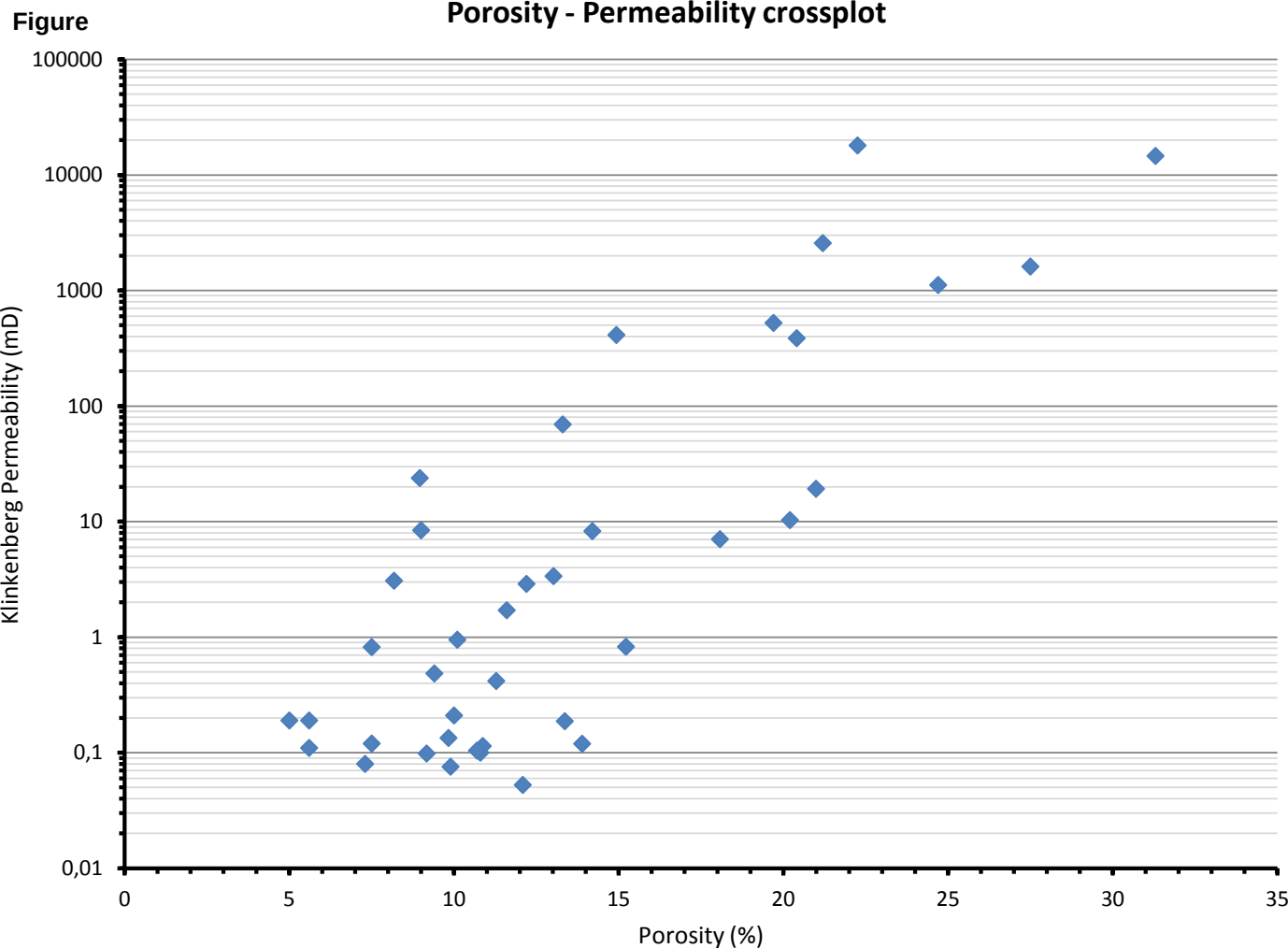
Porosity - Permeability crossplot
Klinkenberg Permeability (mD)
100000
10000
1000
100
10
1
0,1
0,01
0
5
10
15
20
25
30
35
Porosity (%)

Figure

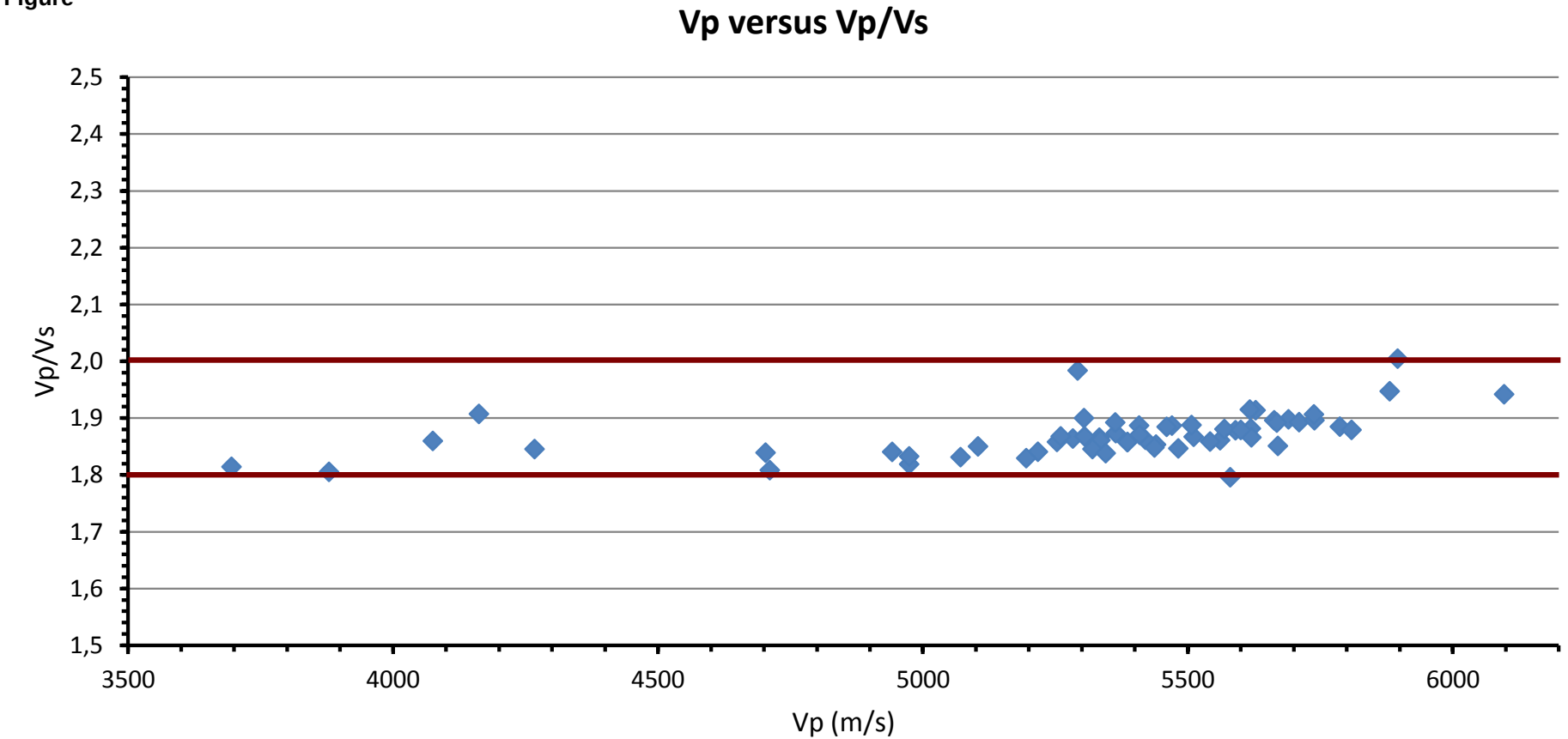
Vp versus Vp/Vs
2,5
2,4
2,3
2,2
2,1
2,0
1,9
1,8
1,7
1,6
1,5
Vp/Vs
3500
4000
4500
5000
5500
6000
Vp (m/s)

Figure

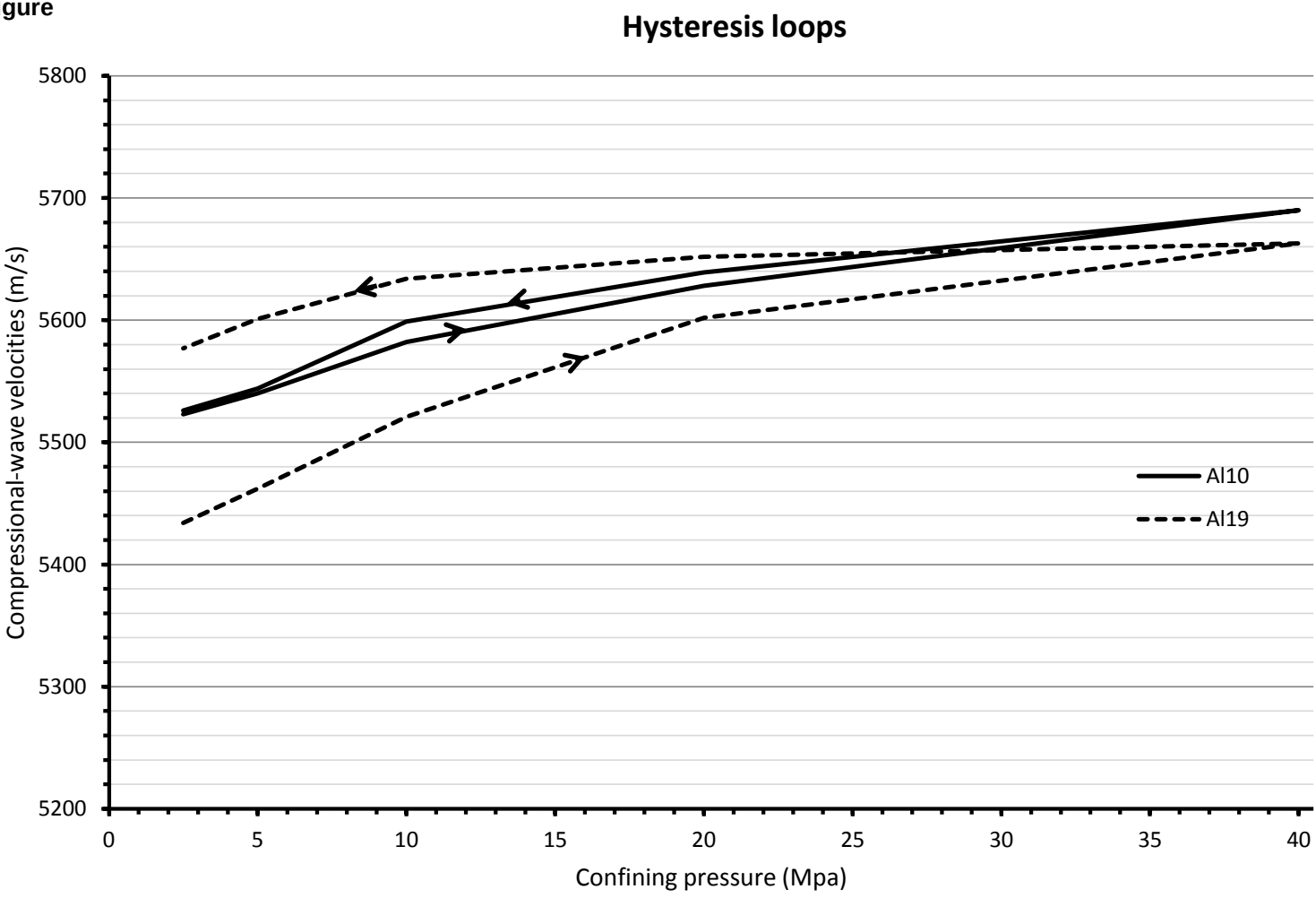
Hysteresis loops
5800
5700
5600
5500
5400
5300
5200
Compressional-wave velocities (m/s)
0
5
10
15
20
25
30
35
40
Confining pressure (Mpa)
Al10
Al19

Figure

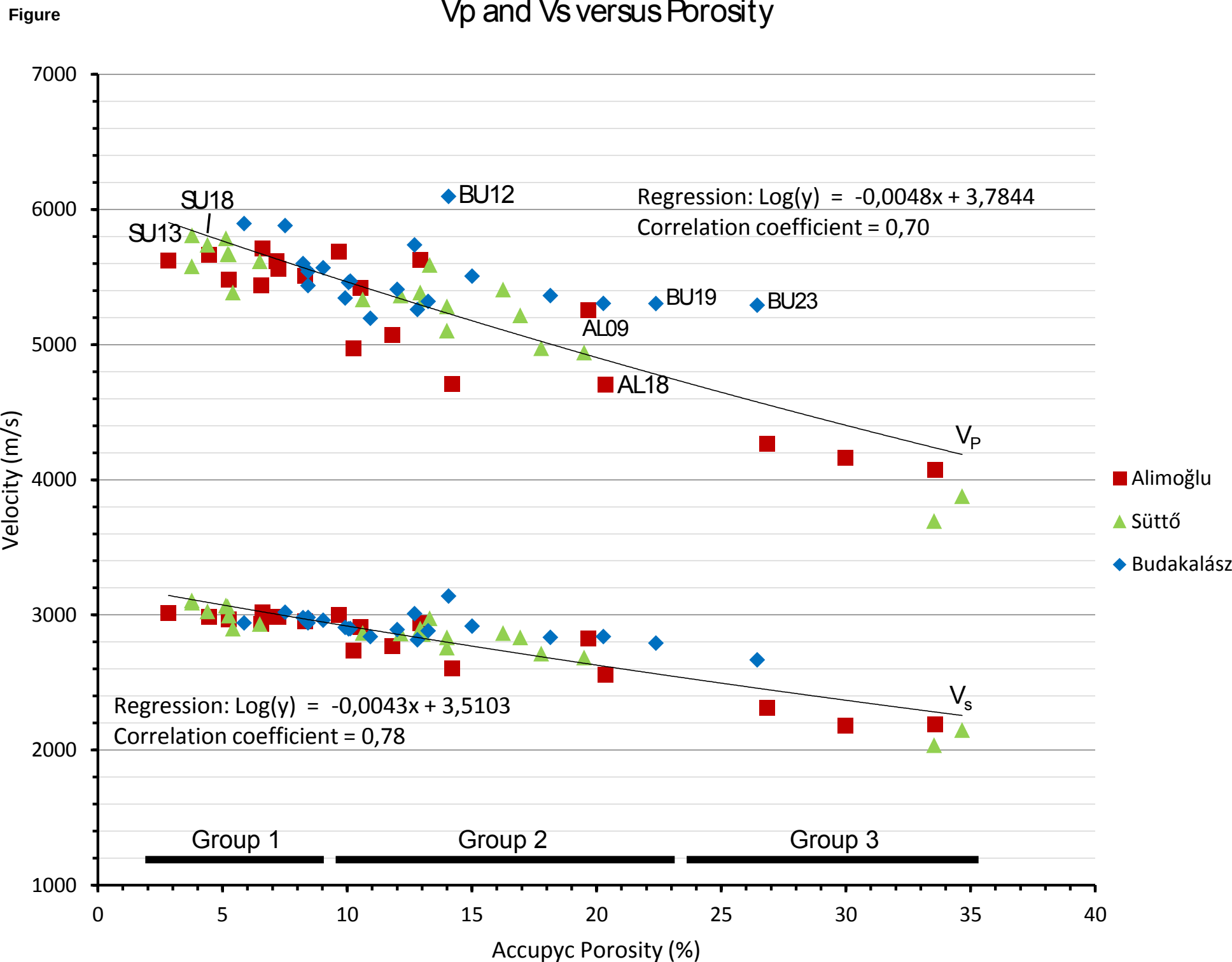
Vp and Vs versus Porosity
Velocity (m/s)
Accupyc Porosity (%)
7000
6000
5000
4000
3000
2000
1000
0
5
10
15
20
25
30
35
40
SU18
SU13
BU12
BU19
BU23
AL09
AL18
Regression: Log(y) = -0,0048x + 3,7844
Correlation coefficient = 0,70
V_P
Regression: Log(y) = -0,0043x + 3,5103
Correlation coefficient = 0,78
V_S
Group 1
Group 2
Group 3
Alimoğlu
Süttő
Budakalász

Figure

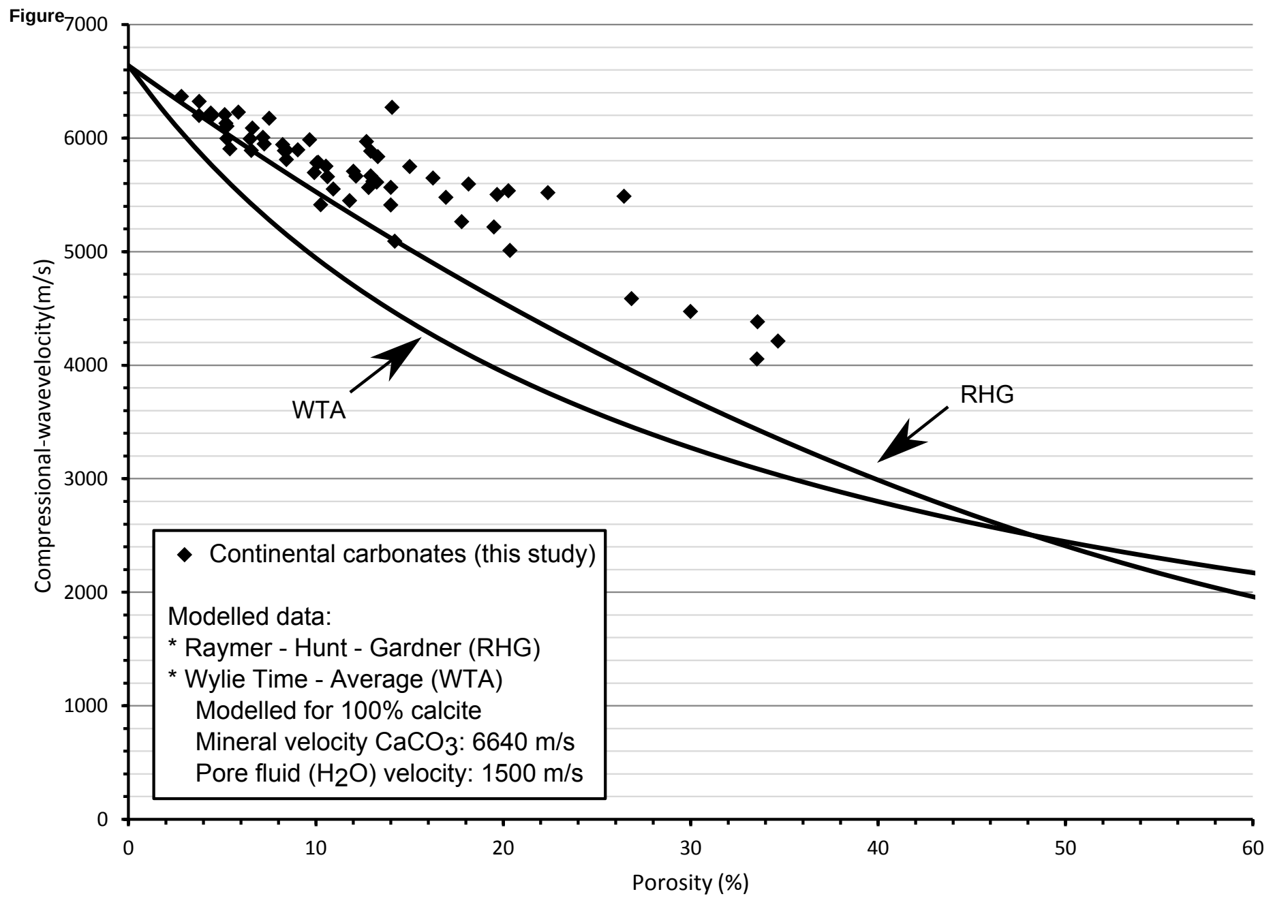
7000
6000
5000
4000
3000
2000
1000
0
Compressional-wavevelocity(m/s)
0
10
20
30
40
50
60
Porosity (%)
WTA
RHG
Continental carbonates (this study)
Modelled data:
* Raymer - Hunt - Gardner (RHG)
* Wylie Time - Average (WTA)
Modelled for 100% calcite
Mineral velocity $CaCO_3$: 6640 m/s
Pore fluid (H_2O) velocity: 1500 m/s

Figure

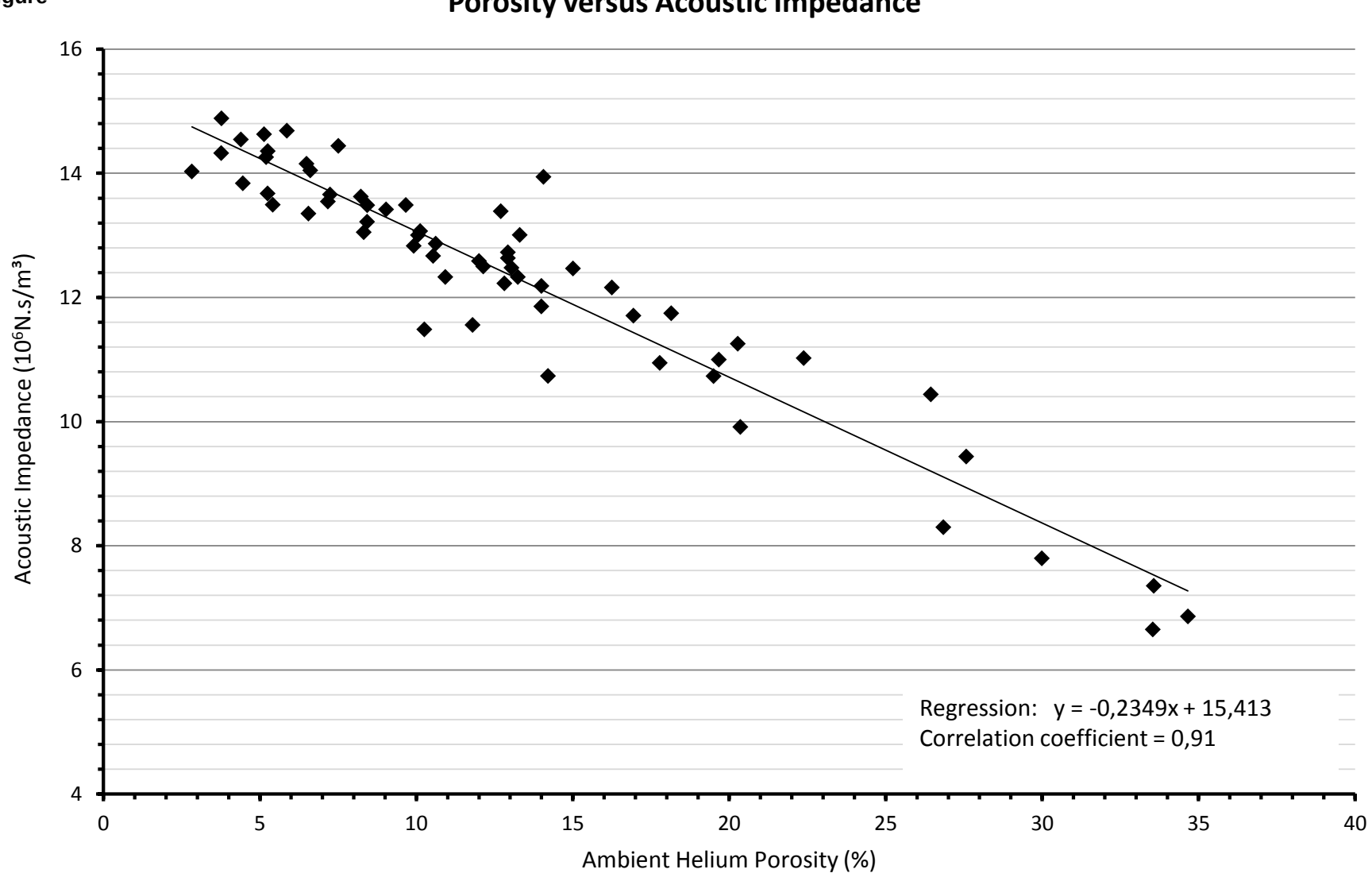
Porosity versus Acoustic Impedance
Acoustic Impedance (10^6N.s/m³)
Ambient Helium Porosity (%)
16
14
12
10
8
6
4
0
5
10
15
20
25
30
35
40
Regression: y = -0,2349x + 15,413
Correlation coefficient = 0,91

Figure

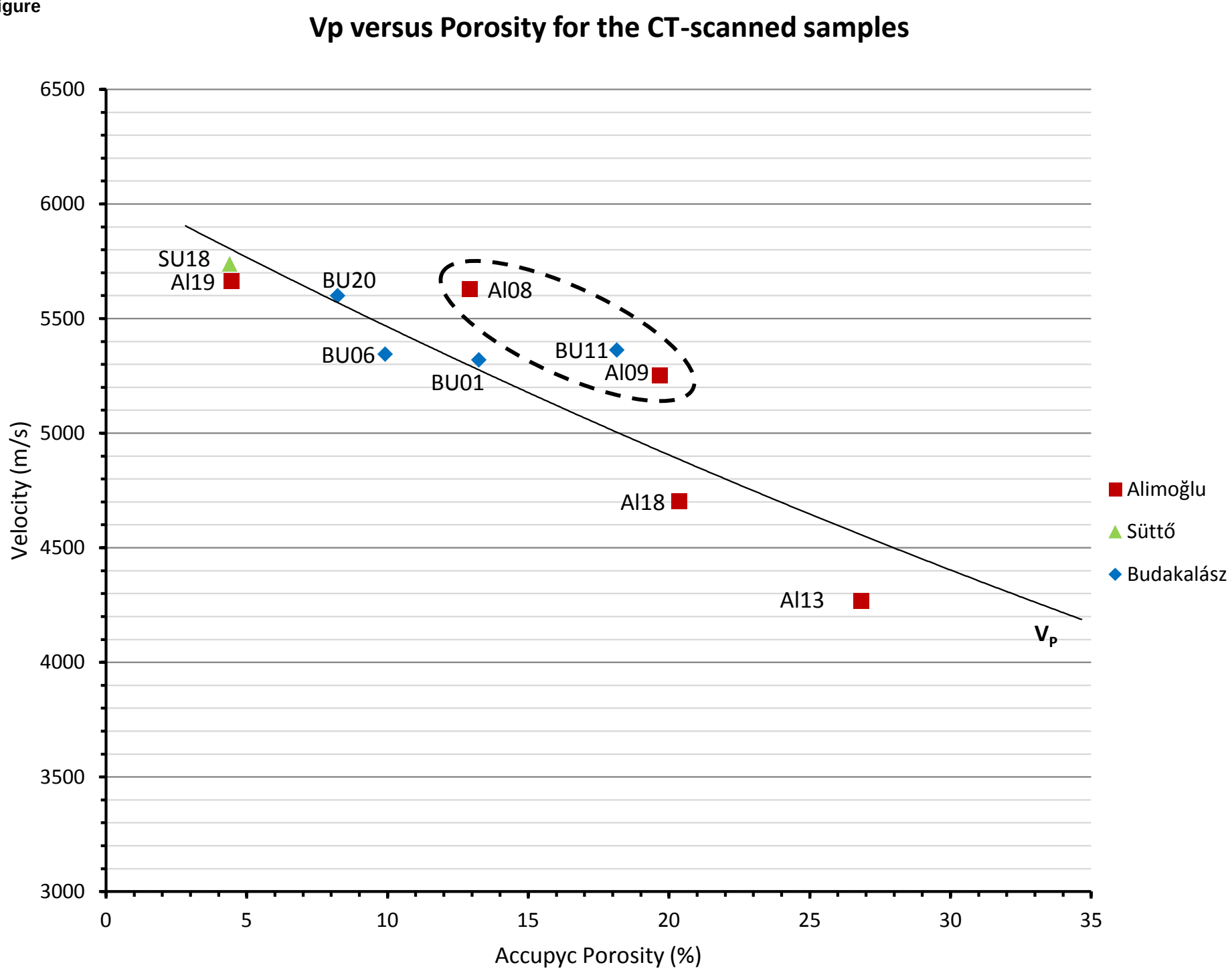
Vp versus Porosity for the CT-scanned samples
6500
6000
5500
5000
4500
4000
3500
3000
Velocity (m/s)
0
5
10
15
20
25
30
35
Accupyc Porosity (%)
SU18
Al19
BU20
Al08
BU06
BU11
Al09
BU01
Al18
Al13
V_P
Alimoğlu
Süttő
Budakalász

Figure

Click here to download high resolution image

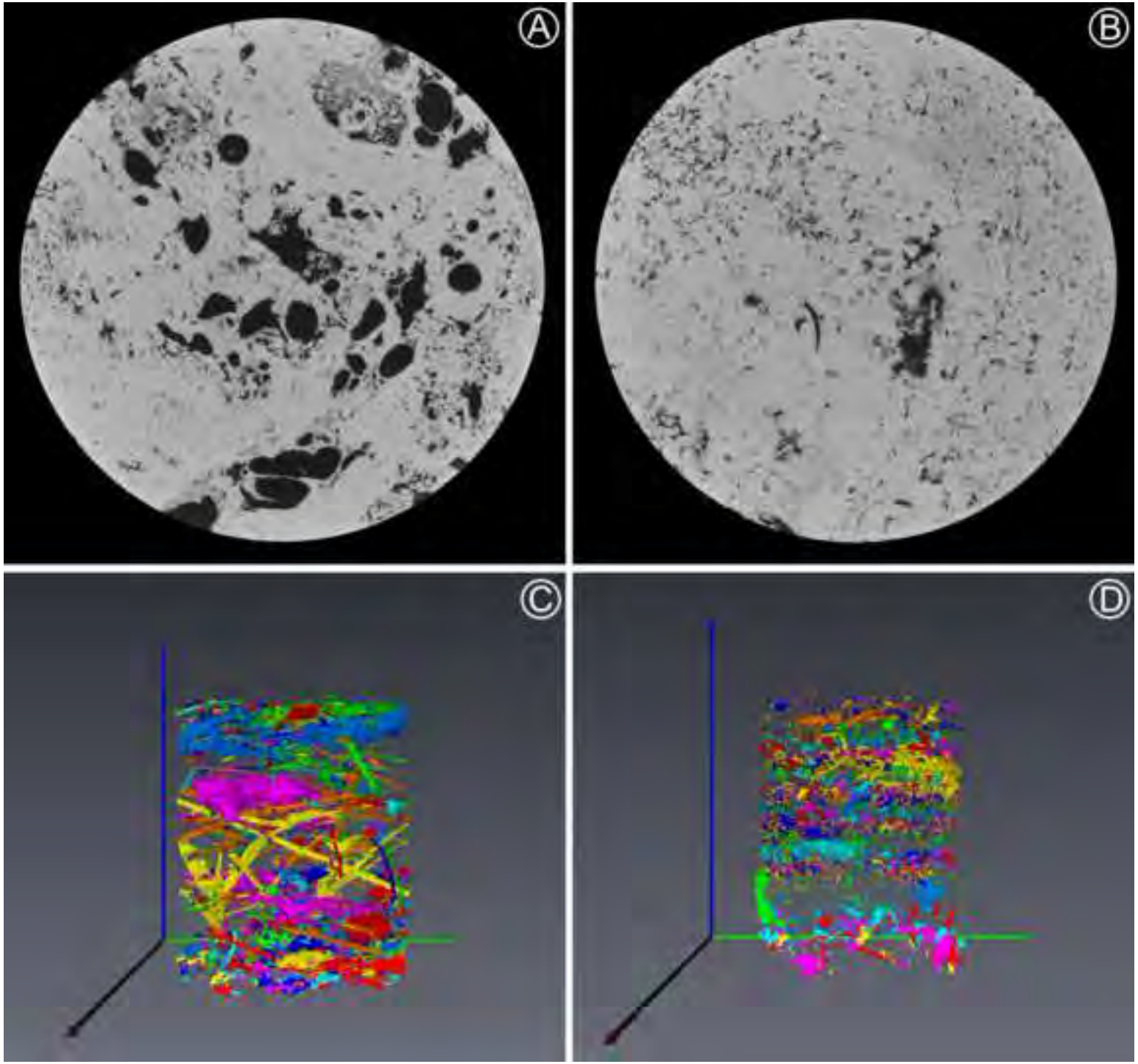

Figure

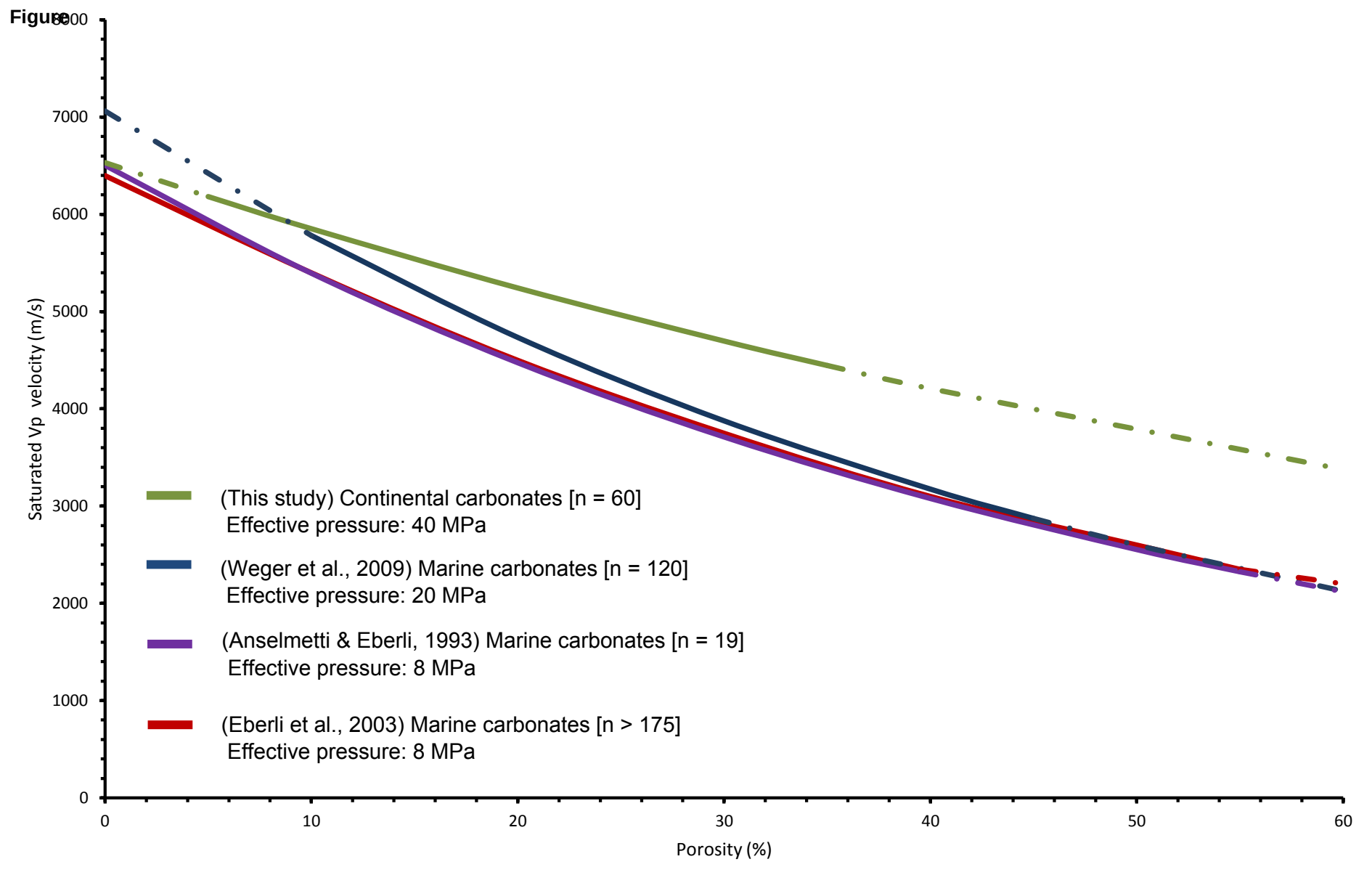
Saturated Vp velocity (m/s)
8000
7000
6000
5000
4000
3000
2000
1000
0
0
10
20
30
40
50
60
Porosity (%)
(This study) Continental carbonates [n = 60]
Effective pressure: 40 MPa
(Weger et al., 2009) Marine carbonates [n = 120]
Effective pressure: 20 MPa
(Anselmetti & Eberli, 1993) Marine carbonates [n = 19]
Effective pressure: 8 MPa
(Eberli et al., 2003) Marine carbonates [n > 175]
Effective pressure: 8 MPa

Table

Table 1. Summary of the conducted petrophysical measurements

Sample	Facies	ρ_d (g/cc)	ρ_s (g/cc)	Accupyc ϕ (%)	Kl. Perm (mD)	V_p (40 Mpa) (m/s)	V_s (40 Mpa) (m/s)	A.I. (10^6 Ns/m³)
Al01	Pool	2,45	2,63	6,5	0,1	5440	2935	13,35
AL02	Pool	2,49	2,63	5,2	0,2	5482	2968	13,68
Al03	Pool	2,41	2,60	7,2	8,4	5619	2986	13,55
Al04	Pool	2,50	2,57	2,8	0,1	5620	3012	14,03
Al05	Casc.	2,34	2,61	10,5	1,7	5420	2911	12,67
Al06	Wfall.	1,80	2,72	33,6	14600,0	4075	2191	7,36
Al08	Reed	2,26	2,60	12,9	69,4	5628	2941	12,73
Al09	Reed	2,09	2,61	19,7	524,0	5253	2827	11,00
Al10	Pool	2,37	2,62	9,7	0,1	5690	2998	13,49
Al11	Pool	2,46	2,63	6,6	0,8	5710	3018	14,05
Al12	Pool	2,46	2,65	7,2	0,1	5561	2988	13,66
Al13	Wfall.	1,94	2,66	26,8	1116,0	4267	2312	8,30
Al14	Wfall.	1,87	2,68	30,0	1611,0	4162	2182	7,80
Al15	Cascade	2,28	2,58	11,8	2,9	5071	2769	11,56
Al16	Cascade	2,31	2,57	10,3	0,2	4974	2735	11,49
Al17	Wfall.	2,28	2,66	14,2	8,3	4711	2605	10,74
Al18	Wfall.	2,11	2,65	20,4	10,3	4703	2557	9,91
Al19	Casc.	2,44	2,56	4,5	0,2	5663	2987	13,84
Al20	Casc.	2,37	2,58	8,3	1,0	5511	2952	13,05
SU01	Pool	2,52	2,65	5,2	/	5670	3063	14,26
SU02	Reed	2,31	2,68	14,0	/	5283	2834	12,19
SU03	Pool	2,53	2,66	5,1	/	5787	3070	14,63
SU04	Reed	2,34	2,69	13,0	/	5333	2859	12,48
SU05	Reed	1,80	2,71	33,5	/	3695	2037	6,65
SU06	Reed	1,77	2,71	34,7	/	3879	2149	6,86
SU07	Pool	2,51	2,65	5,4	/	5386	2899	13,49
SU08	Reed	2,35	2,69	12,9	/	5386	2899	12,64
SU09	Reed	2,25	2,69	16,2	/	5408	2866	12,16
SU10	Reed	2,33	2,65	12,1	/	5364	2863	12,50
SU11	Reed	2,17	2,70	19,5	/	4942	2685	10,73
SU12	Reed	2,24	2,70	16,9	/	5217	2834	11,71
SU13	Pool	2,56	2,66	3,8	/	5809	3091	14,89
SU14	Reed	2,20	2,68	17,8	/	4974	2714	10,95
SU15	Reed	2,33	2,68	13,3	/	5590	2976	13,01
SU16	Pool	2,41	2,70	10,6	/	5335	2867	12,87
SU17	Pool	2,32	2,70	14,0	/	5104	2759	11,86
SU18	Pool	2,53	2,65	4,4	/	5739	3027	14,55
SU19	Pool	2,53	2,67	5,2	/	5668	2996	14,36
SU20	Pook	2,52	2,69	6,5	/	5617	2933	14,15
SU21	Pool	2,57	2,67	3,8	/	5580	3107	14,33
BU01	Pool	2,32	2,67	13,2	0,1	5320	2883	12,33
BU02	Pool	2,33	2,64	12,0	0,2	5409	2892	12,59
BU03	Pool	2,33	2,67	12,7	0,1	5738	3010	13,39
BU04	Pool	2,41	2,65	9,0	0,1	5569	2961	13,42
BU05	Casc.	2,39	2,66	10,1	0,1	5470	2899	13,07
BU06	Casc.	2,40	2,66	9,9	0,1	5345	2908	12,83
BU07	Casc.	2,43	2,66	8,4	0,1	5437	2942	13,22
BU09	Casc.	2,37	2,66	10,9	0,1	5195	2840	12,33
BU10	Casc.	2,26	2,66	15,0	0,8	5507	2917	12,47
BU11	Reed	2,19	2,68	18,1	7,0	5363	2834	11,75
BU12	Reed	2,29	2,66	14,1	412,1	6097	3140	13,94
BU13	Reed	2,43	2,66	8,4	0,5	5542	2982	13,49
BU14	Reed	2,12	2,66	20,3	19,2	5305	2840	11,26
BU15	Reed	2,38	2,65	10,0	0,4	5460	2897	13,01
BU16	Reed	2,32	2,67	12,8	3,4	5260	2816	12,23
BU18	Marl	2,46	2,66	7,5	3,1	5881	3020	14,44
BU19	Reed	2,08	2,68	22,4	18000,0	5304	2792	11,02
BU20	Marl	2,43	2,65	8,2	23,8	5600	2980	13,63
BU21	Marl	2,49	2,65	5,9	/	5896	2941	14,69
BU23	Reed	1,97	2,68	26,4	/	5292	2668	10,44

Table

Table 2. CT based pore type calculations

Sample number	Calculated pore shapes and their respective volumes (vol%)				
	Rod	Blade	Plate	Cube	Cuboid
AL08	35,88	3,84	5,48	5,2	49,53
AL09	2,58	1,05	3,13	6,72	86,49
AL13	9,85	2,56	30,24	34,13	23,36
AL18	23,45	49,85	7,02	3,99	15,63
AL19	10,74	20,73	24,14	14,42	29,91
BU01	3,69	4,4	30,11	21,72	39,99
BU06	5,96	4,75	43,48	15,84	29,88
BU11	31,94	2,84	9,84	28,82	26,55
BU20	11,71	2,63	4,97	68,14	12,52
SU18	7,42	4,42	64,47	9,94	13,71